Materials Today Energy 7 (2018) 246–259

Contents lists available at ScienceDirect

Materials Today Energy

journal homepage: www.journals.elsevier.com/materials-today-energy/

Recent progress on perovskite materials in photovoltaic and water splitting applications

Md Moniruddin [a, 1], Baurzhan Ilyassov [b, c, 1], Xiao Zhao [a], Eric Smith [a], Timur Serikov [b], Niyazbek Ibrayev [b], Ramazan Asmatulu [d], Nurxat Nuraje [a, *]

[a] Department of Chemical Engineering, Texas Tech University, Lubbock, TX79409, USA
[b] Institute of Molecular Nanophotonics, E.A. Buketov Karaganda State University, 100028, Karaganda, Kazakhstan
[c] Solar Energy Laboratory, PI "National Laboratory Astana", Nazarbayev University, 010000, Astana, Kazakhstan
[d] Department of Mechanical Engineering, Wichita State University, Wichita, KS 67260, USA

ARTICLE INFO

Article history:
Received 2 March 2017
Received in revised form
21 September 2017
Accepted 17 October 2017
Available online 14 November 2017

Keywords:
Perovskite solar cell
Water splitting
Methylammonium lead halides
Photovoltaic
Photocatalyst
Photoelectrochemical cell

ABSTRACT

Both inorganic and hybrid (organo-inorganic) perovskite materials are potential candidates as photocatalysts for use in both photovoltaic (PV) and photocatalytic water splitting applications. Currently, research has been focused on specifically designing perovskite materials so they can harness the broad spectrum of the visible light wavelength. Inorganic perovskites such as titanates, tantalates, niobates, and ferrites show great promise as visible light-driven photocatalysts for water splitting, whereas hybrid perovskites such as methylammonium lead halides reveal unique photovoltaic and charge transport properties. The main objective of this article is to examine the progress on some recent research on perovskite nanomaterials for both solar cell and water splitting applications. This mini review paper summarizes some recent developments of organic and inorganic perovskite materials (PMs) and provides useful insights for their future improvement.

1. Introduction

Due to the world's growing population and industrialization, the demand for energy is also increasing. Using fuels as an energy source produces greenhouse gases, which have a detrimental effect on the environment, especially global warming [1–3]. To mitigate this problem, it is important to develop alternative clean energy sources that can fulfill the energy demand. Harnessing energy directly from sunlight is one option to fulfill the need for clean energy and simultaneously have a negligible environmental effect [4]. Solar energy can be utilized in PV applications to generate electricity and to split water to produce hydrogen. Developing suitable photocatalysts for PV [5,6] and water splitting reaction [7], is an important step toward harnessing solar light efficiently.

Organic lead halide perovskites have demonstrated promising applications in renewable energy production. These perovskites show high photon absorptivity in the optical range as well as a sharp band edge implying that the materials have low levels of disorder [8,9]. In addition, they possess long charge-carrier diffusion lengths (>1 μm) in comparison to their incident light absorption depths (~100 nm) [10–14]. These characteristics facilitate the maximum number of photoexcited charge carriers transportation through the electron-hole transporting layers to the electrodes [15–18]. Therefore, organic lead halide perovskites are beneficial in perovskite solar cell (PSCs) to generate electricity.

In the last three years, power conversion efficiencies (PCEs) of PV cells made from perovskites have dramatically jumped from 4% to 22.1% [19–22]. Due to their high efficiency, PSCs are already competing with established thin-film technologies consisting of the inorganic semiconductor cadmium telluride (CdTe) and copper indium gallium selenide (CIGS) [23]. Regardless of progress in making PSCs more efficient, there are some challenges to commercialization, including toxicity of lead ions, long-term instability, and relatively high cost. It is necessary to put effort into improving and optimizing these negatives aspects in order to make PSCs commercially viable.

Unfortunately, one major drawback of solar power is the variability of its intensity. The usefulness of solar power varies, depending on the location, season, and time of day. The direct transformation of solar energy into chemical fuels is a key

* Corresponding author.
E-mail address: nurxat.nuraje@ttu.edu (N. Nuraje).
[1] Contributed equally.

https://doi.org/10.1016/j.mtener.2017.10.005
2468-6069/

technology to addressing the intermittency in renewable energy sources, solving both effective storage and transportation problems. Water photoelectrolysis is an attractive viable technology to convert solar energy into chemical fuels, especially hydrogen, which can be efficiently used in a fuel cell for power generation with only water as by-product [24,25]. Therefore, hydrogen is considered to be a green energy carrier and an effective way to preserve solar energy under no-sunlight conditions. However, to generate hydrogen from water photoelectrolysis, some key factors must be addressed: properly choosing the materials for photocatalysts, designing the photocatalysts, and engineering the water-splitting device. Moreover, a sustainable solar water splitting device should be efficient, economical, and stable over the long term.

In this context, metal oxides have been investigated for their photocatalytic applications, especially titanium (IV) oxide (TiO_2)-based photo catalysts [26–28]. Perovskite materials (PMs) have also garnered major interest in water-splitting applications, due to their unique electrochemical and photophysical properties [29,30]. They have a suitable band gap position in order to perform water splitting, but most of them are photoactive in the ultraviolet (UV) light region. The literature indicates that different design strategies have been followed to utilize the broad spectrum of visible light. One advantage of perovskite is the flexibility to alter its band gap position by adding different elements into the lattice, which ultimately gives a broader scope to the design of its photocatalytic properties [31]. Some perovskite compounds, such as $PbZrO_3$, $BaTiO_3$, and $PbTiO_3$, show piezoelectric properties which can be utilized in designing photocatalysts for water splitting [32,33]. Also, noble metals (Au and Ag) also can be combined with perovskite materials in order to utilize their plasmonic characteristics for designing effective photocatalysts [34,35]. PMs are easy to synthesize and can be produced in different sizes and shapes using different techniques. Details of different PM synthesis techniques have been provided previously [33].

This review paper is intended to examine the recent progress using perovskites for photocatalytic water splitting reactions and PVs. For PVs, emphasis is placed on organolead halide deposition process and operation principal of PSC. For water splitting, this review article is focused on different PM design strategies to capture the visible light and some recent photocatalytic performances of different PMs in water splitting. Based on this context, this review article is organized in five sections. Section 1 introduces the perovskite structure. Section 2, provides a discussion of the recent progress in organolead halide perovskite, the deposition processes of organolead perovskite for solar cells, and the operation principles of PSCs. Section 3 presents the characteristics of PMs and their design strategies, some recent progress of perovskite compounds in using water splitting. Discussion of the fundamentals and design strategies gives readers some insight into PMs for further development. Section 4 is briefly discussed about the degradation phenomena of PMs. Finally, Section 5, a summary of the future prospect of using PMs in water splitting and PV applications.

1.1. Introduction of perovskites materials

Perovskite materials possess the same crystalline unit cell as calcium titanate ($CaTiO_3$). Compounds having a perovskite structure exist widely in the earth, and among them, magnesium silicate ($MgSiO_3$) perovskite is considered to be the most prevalent mineral in the earth [36]. PMs have various intriguing properties and useful applications, including large magnetoresistance, superconductivity, ferroelectricity, transport properties, and optical properties, which can be utilized in designing effective devices for PVs and photocatalysts for water splitting. The perovskite structure shows a formula of ABX_3, where B and X represent a metal ion and an anion (O^{2-}, I^-, Br^-, Cl^-), respectively [37]. As shown in Fig. 1a, B and X form a BX_6 octahedral, where X lies in the corners around B, which is located at the center of the octahedral. The BX_6 octahedral forms a three-dimensional extended system by linking all-corners with each other (Fig. 1b). The symbol A represents a metal cation, which is located in a vacancy within the octahedral and maintains the charge neutrality of the entire network system. The A cations (Ca^{2+}, K^+, Na^+, Sr^{2+}, Pb^{2+}, Ce^{3+}) reside in the 12 coordinated sites between the octahedrals. The position of cation A sites, cation B sites, and anion X sites in the cubic crystalline unit cells are located at the corner (0,0,0), body center (1/2,1/2,1/2) and face center positions (1/2,1/2,0), respectively. Examples of the perovskite structure are $SrTiO_3$ [38] and $CsSnBr_3$ [39].

In most cases, perovskites have a distorted type of cubic structure. These distortions are incredibly large and complicated. Tilting the octahedron leads to a pseudo-cubic structure of the $CaTiO_3$ mineral. According to Cheng et al. [37], the various mechanisms of distortion can be classified into five types: (1) distortion of the BX_6 octahedron; (2) off-center displacement of the B cations in the BX_6, which is responsible for origin of ferroelectricity; (3) tilting of the octahedra, which is typically caused by an A cation since it is too small to be located at the cuboctahedral site; (4) assembling of more than one kind of cation, A or B, or more than one kind of vacancy; and (5) ordering of more than one kind of anion or vacancy. The physical properties of PMs—particularly electronic, optical, transport, magnetic, and dielectric properties—are subject to tremendous distortion. These properties are significant in many applications that use PMs. Therefore, distortions as the result of

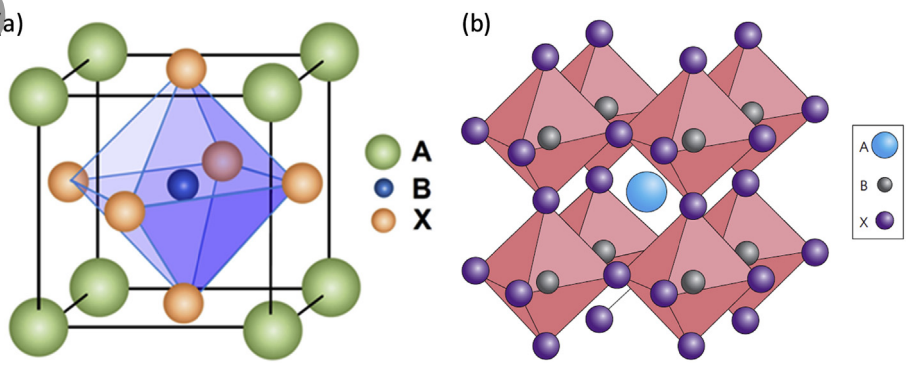

Fig. 1. (a) ABX_3 perovskite unit cell, and (b) extended network structure of perovskites linked via the corner-shared octahedral. Reprinted from Refs. [40,41].

cation substitution can be used for tuning the physical properties given off by perovskites.

2. Perovskite materials for photovoltaics

Typically, the PMs used in solar cells are three-dimensional hybrid perovskites, consisting of organic cations (CH_3NH_{3+}, MA), metal cations (Pb^{2+}), and halides ($X = I^-$, Br^-, Cl^- or mixtures). For efficient devices, the B cation has typically been Pb^{2+}, although Sn^{2+} forms a similar structure with lower and naturally more ideal bandgaps [42], but with lower stability. This section will focus on the $MAPbI_3$ and mixed-halide analog, $MAPbI_{3-x}Cl_x$, perovskite films. In addition, it will present recent progress in organolead halide perovskite and various methods used in the formation of films, and consider the operation principles of perovskite solar cells, which are not yet fully understood.

2.1. Latest progress in organolead halide perovskite for solar cells

In 2013, the journal *Science* reported that one of the top ten breakthroughs of 2013 has become highly efficient organolead halide perovskite solar cells [43]. In PSCs, the organolead halide perovskite, $CH_3NH_3PbX_3$ (where $X = I^-$, Br^-, Cl^-), is used as a photoactive layer to harvest sunlight. The configuration of PSCs is similar to the configuration of dye-sensitized solar cells (DSSCs) [44,45]. In 2009, Kojima et al. [46] first published a report on using perovskite nanoparticles as visible light sensitizers in liquid DSSC based on a mesoporous TiO_2 scaffold yielding efficiencies of 3.81%. However, these first DSSCs sensitized by perovskite nanoparticles had poor stability because of a liquid electrolyte that corrupts the perovskite sensitizer. Later, Kim et al. [21] also used the perovskite nanoparticles to sensitize TiO_2 films in a solar cell and delivered PCE of up to 9.7%. They used hole-conductor spiro-MeOTAD instead of liquid electrolyte. Shortly after that, D'innocenzo et al. [47] employed mesoporous Al_2O_3 as a scaffold and a mixed halide perovskite, $CH_3NH_3PbI_{3-x}Cl_x$, as a sunlight absorber. The insulting Al_2O_3 scaffold supported the formation of continuous thin films of $CH_3NH_3PbI_{3-x}Cl_x$ and dramatically decreased the energy costs need due to splitting excitons (photoinduced electron-hole pairs) as well as isolating free charges from disordered networks such as mesoporous TiO_2(mp-TiO_2). The "meso-superstructure" PSC had a PCE as high as 10.9% and generated 1.1 V of open-circuit photovoltage [19]. This study, for the first time, demonstrated that mixed PMs can be used as a sunlight absorber in addition to a charge carrier conductor. The PCE of this cell was boosted up to 12% by infiltration of the TiO_2 film pores with $CH_3NH_3PbI_3$ perovskite and overlayers of $CH_3NH_3PbI_3$ co-existing on top of the mp-TiO_2 film [48]. This study indicated that the perovskite performs a double role as light harvester and hole conductor.

A significant improvement in the PSC fabrication is that its performance and reproducibility was achieved by introducing a two-step sequential deposition technique. Lead (II) iodide (PbI_2) was first added to a mp-TiO_2 film and then converted into the perovskite by adding of CH_3NH_3I, which leads to a cell with a PCE of 15% [49]. Furthermore, Liu et al. [50] showed that it is not necessary to use nanostructuring to attain high efficiencies for the same material. They obtained a 15% PCE in a simple planar heterojunction structure by applying vapor-deposited perovskite as the absorbing layer, an n-type TiO_2 as an electron-collecting layer, and spiro-MeOTAD as a p-type hole transporter. This study demonstrated that the highest efficiencies can come from these perovskite absorbers, even without the use of complex nanostructures. Zhou et al. [20] reported 19.3% of PCE for a planar PSC using interface engineering techniques. They inhibited the recombination of photoexcited carriers in the absorber, enabled charge injection into the transport layers, and kept excellent charge removal at the electrodes by tuning the formation of the perovskite layer and cautiously selecting materials. Lately, a certified PSC with 20% PCE has been reported [51], which is an excellent competitor of silicon-based solar cells.

2.2. Deposition processes of organolead perovskite for solar cells

In the first reports on $CH_3NH_3PbI_3$ and $CH_3NH_3PbI_{3-x}Cl_x$ solar cells, the spin-coating technique was used to prepare photoactive absorbers from a sole precursor. A solution of CH_3NH_3I and PbI_2 (stoichiometric ratio) in polar media, such as dimethylformamide (DMF), was used to form $CH_3NH_3PbI_3$ films [21,48]. For forming $CH_3NH_3PbI_{3-x}Cl_x$, a solution of $PbCl_2$ and CH_3NH_3I (molar ratio of 1:3) in DMF was typically used [19,52]. The perovskite absorber can be produced either inside the mesoporous layers or formed as uniform films on TiO_2 compact layers in the case of planar solar cells by proper monitoring of the precursor concentration and spin-coating conditions. For planar cells, the deposition of a uniform perovskite layer by spin-coating demands that variables, including post-deposition treatment, be controlled [53–55]. Since wettability of the underlying layer is different, the deposition of perovskite must be separately optimized for each of layers. The degree of infiltration within the mesoporous layer essentially depends upon the solution concentration, spin-coating rate, and solvent properties. Surface roughness that causes shunts in the PSCs depends on the tendency of perovskite films to crystallize [48]. An important

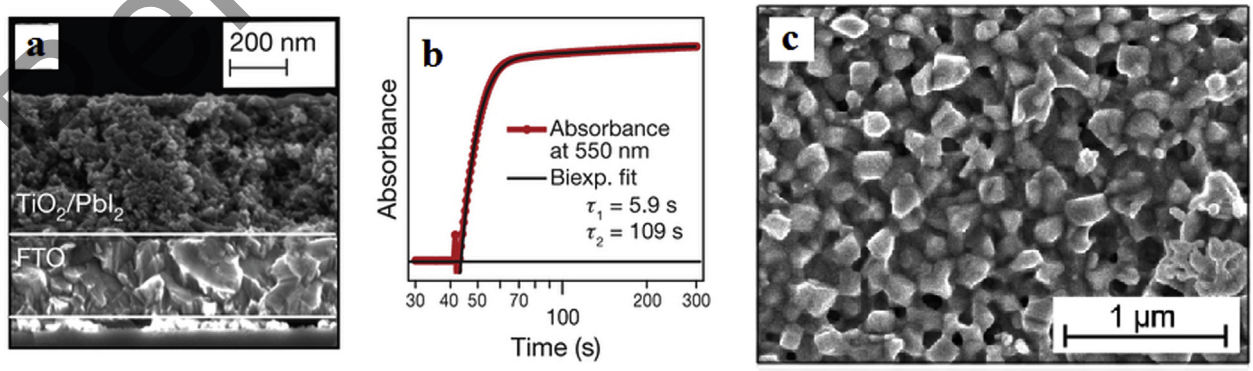

Fig. 2. (a) SEM image (cross-sectional) of mp-TiO_2 film infiltrated with PbI_2, (b) change in film absorbance during transformation of PbI_2 to $CH_3NH_3PbI_3$, and (c) SEM top view of $CH_3NH_3PbI_3$ film prepared utilizing sequential deposition method. Reprinted from Ref. [49].

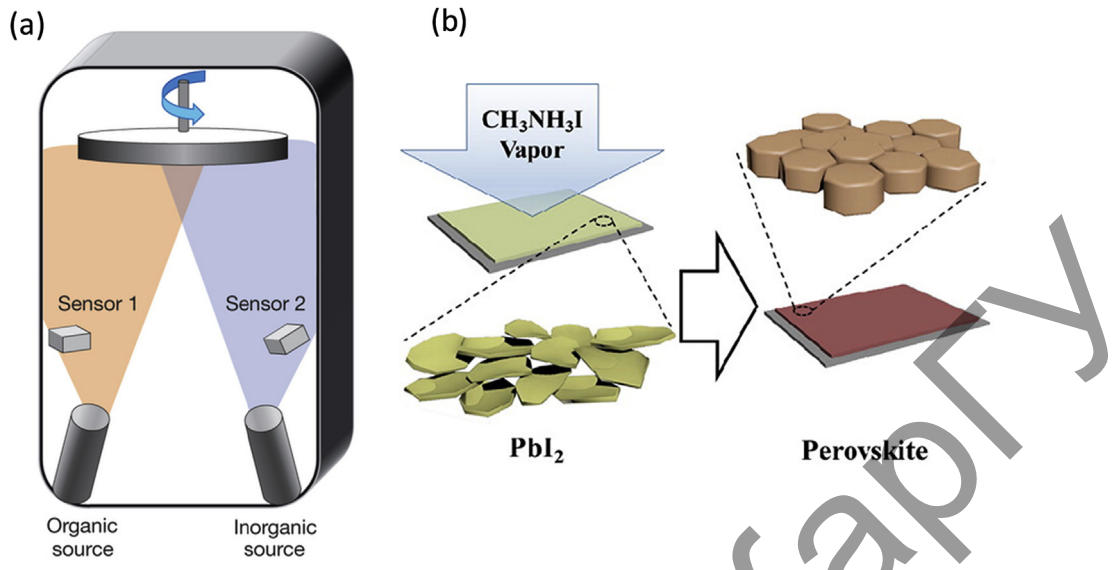

Fig. 3. (a) Schematic of dual-source thermal evaporation equipment, and (b) schematic of PbI_2 conversion to $CH_3NH_3PbI_3$ by exposure to CH_3NH_3I vapor. Reproduced from Ref. [58].

achievement in solution-based deposition is the development of the consecutive deposition method for use in the preparation of PSCs by Burschka et al. [49]. This deposition method is composed of spin-coating a PbI_2 layer onto the TiO_2 mesoporous layer from a solution under proper conditions, solution concentration, spin-coating rate, etc., which allows the PbI_2 to qualitatively infiltrate within the mesoporous layer (first step) (Fig. 2a). Subsequently, the substrates with formed PbI_2, which are yellow in color, are dipped in a CH_3NH_3I solution in a 2-propanol solvent. During this time, the yellow PbI_2 layer is converted into forming the dark brown $CH_3NH_3PbI_3$ within a few seconds [49]. Fig. 2b shows that the increase in absorption at 550 nm is reached within a few seconds of incubating the PbI_2-loaded TiO_2 film to the CH_3NH_3I solution. It is worthwhile mentioning that the conversion time is related to the PbI_2 deposition conditions. This has been reported to be a 20-min conversion time [56], although the original work by Liang et al. [57] indicated that the conversion took 1–3 h. It is likely that the conversion reaction speed is increased because the PbI_2 layer on top of the mesoporous layer has become rougher [49]. The transformation of PbI_2 into $CH_3NH_3PbI_3$ occurred with volume expansion (~75%) [58]. Therefore, a better explanation is that the mesoporous layer is infiltrated by the sequential deposition process. The scanning electron microscopy (SEM) top view of samples deposited by these process shows a highly crystalline film with complete coverage (Fig. 2c).

Vapor deposition is another method that is typically utilized to make PSCs along with the extensively applied solution-based deposition processes. Planar PSCs (15.4%) of $CH_3NH_3PbI_{3-x}Cl_x$, produced by evaporation of $PbCl_2$ and CH_3NH_3I from dual evaporation sources (Fig. 3a) were created by Liu et al. [50]. The evaporated perovskite film was sandwiched between a compact TiO_2 and a spin-coated spiro-OMeTAD layers which are performed separately as electron and hole carriers. The deposited perovskite films were very uniform and compact and had crystal grains of hundreds of nanometers. Using these vapor deposition techniques, Malinkiewicz et al. [59] successfully fabricated a device with 12.04% efficiency utilizing different electron and hole transporters, such as PCBM and PEDOT:PSS. In both cases, in order to produce the desired layers of perovskite and efficient solar cells, a careful optimization of the dual source evaporation process was required. Chen et al. [58] demonstrated a combined approach utilizing vapor phase transformation and solution-based deposition. In this vapor-assisted solution process (VASP), a PbI_2 solution was first spin-coated onto a TiO_2 substrate. Next, the yellow colored films were exposed to CH_3NH_3I at 150 °C in N_2 for 2 h (Fig. 3d). Due to the slow rate of conversion, VASP produced $CH_3NH_3PbI_3$ films with micron sized grains and a low surface roughness (~20 nm). PSCs fabricated from these films had a PCE of 12.1%.

2.3. Operation principles of PSCs

As mentioned previously, the perovskite nanoparticles were initially used to sensitize the porous TiO_2 scaffold. The intended role of the perovskite nanoparticles in the device is similar to that of the dye molecules in a dye-sensitized solar cell. After sunlight is harvested by the perovskite, generated electrons are transported to the perovskite/TiO_2 interface and injected to the conduction band of the TiO_2. The remaining holes are then removed by a redox electrolyte or a solid-state hole-transport material, and further moved to a platinum cathode [60] (Fig. 4a). Further studies revealed that bulk perovskite can act as both a hole and electron transport media, and a thin perovskite film with a thickness of a few hundred

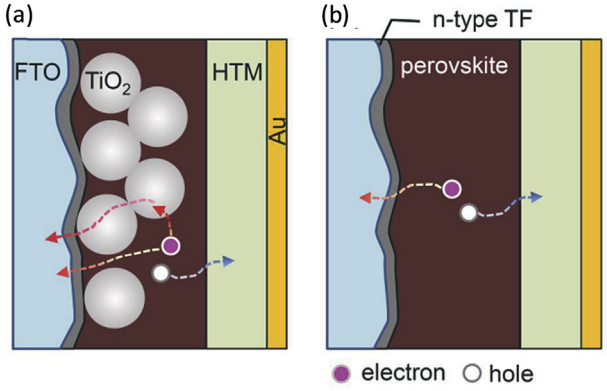

Fig. 4. (a) Mesoscopic PSC with porous TiO_2 scaffold, and (b) planar configuration without TiO_2 scaffold. Fluorine-doped tin oxide (FTO) layer is block layer, n-type semiconductor. HTM layer is hole-transporting material. Reprinted from Ref. [67].

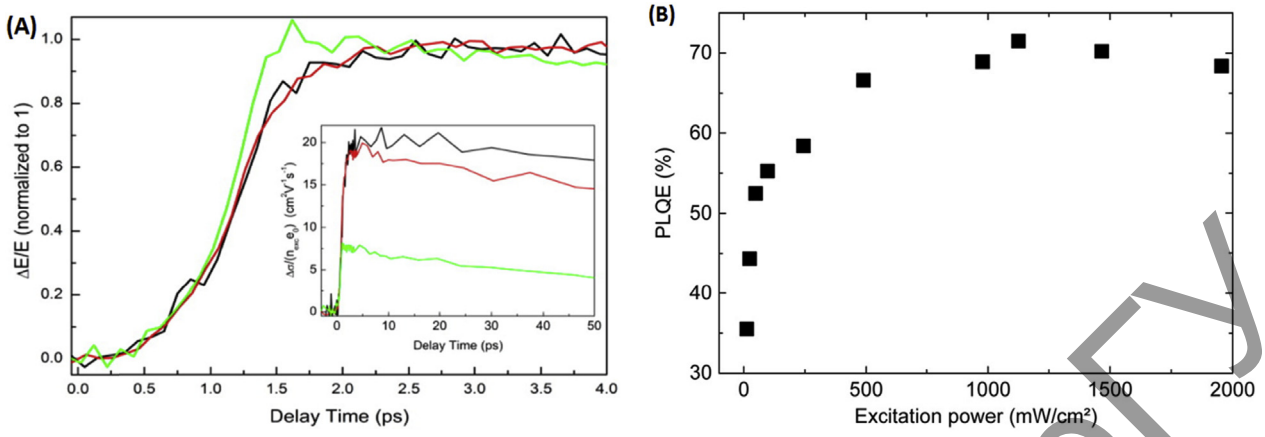

Fig. 5. (A) Time-resolved spectra obtained by pulsed photoexcitation at 400 nm: normalized early time terahertz dynamics of neat $MAPbI_3$ (black), MAPbI3/mesoporous Al_2O_3 (red), and $MAPbI_3$/mesoporous TiO_2 (green) films. Inset shows THz photoconductivity kinetics [72]; (B) photoluminescence quantum efficiency (PLQE) of perovskite thin-film vs excitation power [71]. (For interpretation of the references to colour in this figure legend, the reader is referred to the web version of this article.)

nanometers could even perform charge generation and transport [19,50,52,61,62]. The cell architectures places the perovskite layer between p-type and n-type selective contacts, similar to a planar heterojunction architecture [19] (Fig. 4b). This simple planar architecture, which can be assembled by different preparation methods, has strongly attracted the attention of the photovoltaic community [59,63–66].

In planar perovskite solar cells, the charge generation mechanism and dynamics are not completely clear. The photoexcited species, free electrons and holes, or bound excitons are not completely understood. At room temperature, the upper bound of the exciton binding energy in the perovskite materials with a tetragonal phase is ~50 meV [47]. However, in these computations, the dielectric constant is supposed to be 6.5, but according to Even et al. [68], the effective dielectric constant is probably much greater. In that case, the exciton binding energy in the tetragonal phase is probably ~1–10 meV [68]. Although even for the exciton binding energy of ~50 meV, free charge carriers are generated spontaneously after light harvesting, corresponding to a large concentration of bound excitons [69,70]. According to ultrafast spectroscopy studies (Fig. 5A), dissociation of the exciton occurs during 2 ps after photoexcitation [71,72]. Confirmation of this feature requires a thorough interpretation of the transient spectra. Mobilities of the free electrons and holes are approximately equal and lie in the range ~10–30 $cm^2\ V^{-1}\ s^{-1}$ (Fig. 5A inset) [13,72,73]. Stranks et al. [70] studied recombination processes in organic-inorganic perovskite under high light intensities, and found that recombination occurs by means of a bimolecular mechanism, thus indicating that the prevalent relaxation pathway is a recombination of both free electrons and holes [74]. The recombination in these perovskites is mainly radiative as well. Quantum efficiencies of photoluminescence reaches values of 70% at room temperature (Fig. 5B), [70,71] and even 100% at low temperature [14]. These high luminescence efficiency attributes perovskite solar cells to the efficiency limit of Shockley–Queisser. In that case, all recombination is presumed to be radiative [75–77].

In the case of planar heterojunction cells, it is known that the crucial prerequisite for proper operation of the cell is that diffusion lengths of the electron and hole must be greater than the photoactive layer thickness needed to achieve entire incident light harvesting. The diffusion length is estimated to be greater than 1 μm for both charge carriers (electrons and holes) in the $MAPbI_3$–xClx layer (Fig. 5B) [10,11]. This value is appropriately long for the efficient operation of a cell with planar heterojunction architecture as

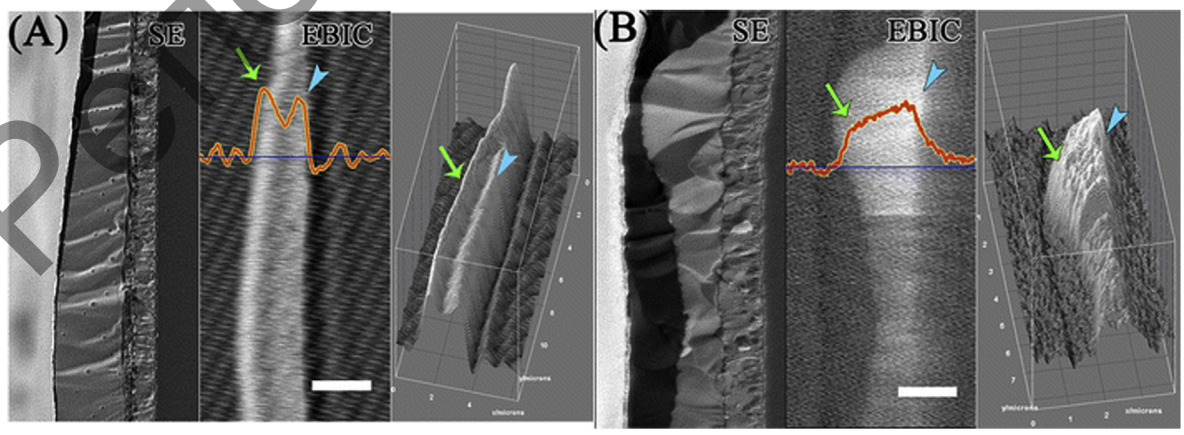

Fig. 6. SE and EBIC images of cross sections of $CH_3NH_3PbI_{3-x}Cl_x$ (A) (scale bar 2 μm) and $CH_3NH_3PbI_3$ (B) planar solar cells (scale bar 1 μm). Scans were taken at the lines' positions. Arrows show peaks for I–Cl and where peaks are in the case of pure iodide. Right panels are 3D surface plots of EBIC images. Ripples observed in EBIC image of (A) outside (semi-) conductive regions are due to background noise. Reprinted from Ref. [62].

because an absorption depth is about 400 nm at a light wavelength of 700 nm [53,61,78]. The long diffusion length is explained by a long lifetime of charge carriers on the order of 300 ns to μs [10].

The electron-beam induced current (EBIC) mapping technique has been used to determine the operating principal of planar PSCs. EBIC data revealed that the operating principal is similar to that of a thin-film solar cell [14,62]. In EBIC scans (Fig. 6A,B), two peaks are consistent with p–i–n operation [70] are observed. These results imply that the most probable operating method is that the photon is absorbed, and free charge carriers are generated at room temperature [47,74]. Furthermore, generated charge carriers move through the perovskite film and selectively pass across their respective electrodes where they promote the current in the external circuit [62].

The charge carrier diffusion lengths calculated by EBIC are approximately 2 μm for the I/Cl mixed halide perovskite and 1 μm for the triiodide perovskite during hole diffusion. This result is consistent with carrier diffusion lengths examined by terahertz time-domain spectroscopy [13]. However, these lengths are longer than those estimated by time-resolved photoluminescence quenching measurements [10,11]. Photoluminescence quenching measurements will tend to give an underestimate since they assume perfect quenching and homogenous recombination within the bulk of the film.

The perovskite film morphology and the defect density within the films strongly influence on the charge carrier lifetime in the perovskite. According to recent research on single crystals of $MAPbI_3$ and $MAPbBr_3$, defect densities in such crystals are lower ~10^{10} cm^{-3} [79,80], in comparison to those in polycrystalline perovskite films, which are ~10^{16} cm^{-3} [69,78]. In these single crystals, an estimated charge carrier lifetime and a corresponding charge carrier diffusion length reach value of a few hundred microseconds and of 175 μm, respectively. In order to estimate the lifetime of the charge carrier, photovoltage decay and electrochemical impedance spectroscopy techniques of electronically contacted crystals were used. If the charge carrier trapping takes place at the crystal surface, then it may overestimate the lifetime of the charge carrier, which case, the results must be verified by other techniques.

In polycrystalline thin films, the intergrain potential barriers create obstacles to carrier transport through the layer and may reduce mobility of the carrier by many orders of magnitude from that found in a single-crystal material. In this respect, CIGS has long been regarded as a “better material” since it has an extremely low intergrain potential barrier of 100 meV [14]. In comparison with CIGS, the intergrain potential barrier at the CdTe grain boundaries, depending on processing conditions, is ~100–800 meV [14]. However, the intergrain potential barrier in polycrystalline $MAPbI_3$ perovskite films in the dark is only ~45 meV and further decreases under illumination [62]. This implies that charge trapping at the grain boundaries in perovskite films must be much less of an obstacle than in CIGS or CdTe. However, cells with large grain size had a better drive performance as well as enhanced diffusion length for the charge carrier. This implies that the grain boundaries may not be benign [79,80].

Since perovskite films have a high absorption coefficient as well as a sharp absorption edge, it is possible to characterize the energetic disorder by analyzing the exponential dwindling of the absorption spectra below the bandgap with a characteristic energy, or Urbach energy [8,9]. The steepness of the edge of the absorption spectrum indicates the materials quality. Plus, it has a low Urbach energy of 15 meV which indicates a low degree of disorder [48,81]. In comparison, values of Urbach energy of GaAs, CdTe, crystalline silicon, $MAPbI_3$ or $MAPbI_3$–xClx, and CIGS are 7, 10, 11, 15, and 25 meV, respectively. The Urbach energy of perovskite is less than that of CIGS (~25 meV) [48] and somewhat greater than that of GaAs (~7 meV) [8,76]. Regardless, perovskite samples made using the most standard solution-processing methods [73,78] still have low density electronic trap states (~10^{16} cm^{-3}) in the band gap, which strongly influence on the recombination dynamic, cell photovoltage, and photoluminescence quantum efficiencies [70,73] (Fig. 6B).

The most efficient PSC cell is composed of a thin (~200 nm) layer of nanoporous TiO_2 infiltrated and covered with a solid perovskite layer (~200–300 nm) (Fig. 4a) [81–83]. In these nanoporous TiO_2-based perovskite cells, a bottom layer of TiO_2/perovskite performs the role of a bulk distributed heterojunction and a top layer of the perovskite and the hole-transport material operates as a planar heterojunction. Snaith et al. [84] assumed that while proper control of the interfacial surface of the perovskite and the compact n-type layers is reached, the privileged solar cell architecture can be the planar heterojunction one (Fig. 4b).

3. Perovskite materials for water splitting

Several photocatalysts, such as binary and ternary metal oxide, sulphide, phosphide, and nitride compounds, which have been tested for water splitting [85–90]. However, there is still a major challenge to find a champion material that has a suitable band edge potential with smaller band gap for the overall water splitting reaction. In addition, there are also some major issues in designing a good photocatalyst including electron-hole pair recombination and material instability due to photodegradation in photocatalytic water splitting. Perovskites-based compounds are one type of metal oxides photocatalysts that has been widely studied for photocatalytic hydrogen generation from water splitting. Perovskites offer distinct advantages over other classes of materials studied. First, several perovskites offer suitable band edge potentials which are favorable for either the cathodic hydrogen evolution reaction or the anodic oxygen evolution reaction and are also stable in water. Second, the flexibility of A site or B site cation doping in the lattice perovskite can alter its structure, resulting in a significant change in the photophysical properties. Third, ferroelectric and/or piezoelectric properties of perovskites also have the potential to improve their photocatalytic activities [91]. Hence, perovskites are considered a potential photocatalyst for the water splitting reaction [92]. Most perovskites have a high band gap energy thus exhibiting good photocatalytic activity under the UV region alone. Many research studies have been conducted to extend this photocatalytic activity towards the visible light region for water splitting reaction. In Section 3.2 and 3.3, some PM design strategies and their recent photocatalytic performances for water splitting reaction under visible light are briefly discussed.

3.1. Fundamentals of water splitting

The water-splitting reaction is nonspontaneous, whereby the Gibbs free energy change is 237.3 kJ/mol^{-1} at standard temperature and pressure [93]. Therefore, a photocatalyst needs to absorb photon energies from solar light to overcome this thermodynamic limitation of the water-decomposition reaction. The water splitting reaction is a four-electron transport process in which water decomposes into oxygen and hydrogen. To split water into hydrogen and oxygen using sunlight, the photocatalyst must full fill two essential criteria: (a) it must absorb the minimum photon energy of 1.23 eV, which is equivalent to the light wavelength of 1100 nm, and (b) the conduction band (CB) potential of the photocatalyst must be more negative than the redox potential of H^+/H_2 (0 V vs NHE at pH = 0), and the valence band (VB) potential must be more positive than the redox potential of O_2/H_2O (1.23 V vs NHE at pH = 0) [31]. In

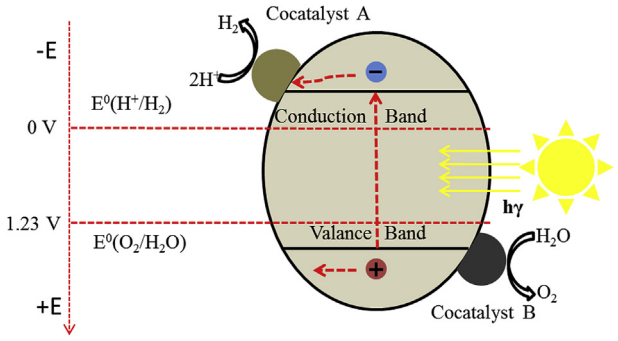

Fig. 7. Steps in overall water splitting mechanism on a heterogeneous photocatalyst.

general, the photocatalyst absorbs light and generates electron-hole pairs under irradiation. The excited electron is then moved to the conduction band and reduces the water to form hydrogen gas. Simultaneously, the hole in the VB oxidizes water into oxygen gas. Steps involved in the water-splitting reaction are depicted in Fig. 7.

3.2. Strategies to design perovskite materials

The effectiveness of a photocatalyst in photocatalytic water splitting depends on three major steps: (a) photon absorption from incident light and generation of electron-hole pairs, (b) separation and transport of photoexcited carriers to the surface active sites, and (c) consumption of photoexcited electron-holes by water redox reactions on the active site [94]. However, most perovskite materials such as titanates or tantalates (>3 eV) have a large band gap energy and thus are not capable of harnessing the major portion of the solar spectrum (visible range) that reaches the earth's surface. Different designs of PMs can increase the visible light absorption, minimize the charge recombination, and enhance the charge separation. In the literature, several strategies have been investigated to design PMs to improve the photocatalytic activity in water splitting. Here, we discuss some key strategies, including the following: (a) band gap engineering to achieve the suitable band edge position, (b) reduction in electron-hole pair recombination by changing particle size and crystal nanostructure, (c) use of plasmonic metal nanoparticles (Au or Ag) to enhance the visible light absorption, (d) development of different heterojunction assemblies to enhance charge separation, and (e) introduction of ferroelectric material to capitalize on its polarization field towards photoexcited charge separation.

3.2.1. Band gap engineering

The electronic band structures of a photocatalyst can be engineered by doping a foreign element into a perovskite structure. The dopant may form a new mid-gap state between the VB and CB or alter the VB or CB position through the mixing of energy levels of the dopant and host elements [95,96]. Generally, with perovskite materials, the bottom edge of the CB and top edge of the VB energy levels are more negative than 0 V and more positive than 3 V, respectively. The CB mainly consists of d^0 transition metal orbitals, and the VB consists of O 2p atomic orbitals. Therefore, by doping suitable elements in the perovskite structure, it is possible to introduce new p or d orbitals in either the VB or CB, respectively, which helps to manipulate the band gap energy to the visible range. For example, the band gap of $SrTiO_3$ is 3.2 eV, but when it is doped with Rh, the band gap is reduced, apparently resulting in H_2 evolution from water splitting under visible light irradiation [97]. Here, Rh is doped as a B-site element (Ti^{4+}) to manipulate the band gap energy of $SrTiO_3$. The dopant exists both in a trivalent ion (Rh^{3+}) and tetravalent (Rh^{4+}) form. Rh^{3+} introduces a donor level at a smaller potential than the top edge of the VB, and this donor level provides the excited electron to the $SrTiO_3$ CB; thus the band gap shrinks apparently [95]. Rh^{4+} creates a new acceptor level, and the excited electron transfers from the VB of the $SrTiO_3$ to the new acceptor level. On the other hand, Zn can be doped as A-site elements to manipulate the band gap energy of $SrTiO_3$. In the Zn-doped- $SrTiO_3$, the VBs dominantly consist of O 2p orbitals, whereas the Zn 3d orbital mainly contributes to the bottom edge of the CBs at a lower negative potential compared to the Ti 3d orbital and results in shrinkage of the band gap [98].

Anion doping at the O-site of perovskites is another potential way to convert UV active catalysts to visible active catalyst for water splitting [99]. A theoretical calculation using DFT and HSE06 has shown that anion doping (N and S) at the O-site of $NaTaO_3$ reduces the band gap significantly since the p orbital energies of anionic elements are higher than the O 2p orbitals. In the S-doping case, new S 3p orbitals form above the VB, which is located at the lower potential of the O 2p orbitals, and results in the VB moving in an upward direction [100]. A recent experimental study has shown that S-doped $NaTaO_3$ exhibits remarkably improved visible-light photocatalytic activity, compared to pure $NaTaO_3$ in photocatalytic degradation of an organic compound [101].

3.2.2. Varying crystal structure and particle morphology

Particle morphologies, including crystal structure and size, crystallinity, and particle structure of perovskite photocatalysts, significantly influence the photocatalytic activity. Although changing the particle morphologies may not make the perovskite photocatalysts active in visible light, it can help to improve the photoexcited charge separation efficiency, which is one of the major hindrances toward designing efficient photocatalysts for water splitting. The photoelectron excitation and transfer process can be improved by restructuring the crystal structure of the perovskite photocatalysts to enhance the photocatalytic activity. For example, $NaNbO_3$ has two different crystal structures, cubic and orthorhombic, with band gap energies of 3.29 eV and 3.45 eV, respectively. Cubic $NaNbO_3$ exhibited two times higher H_2 evolution than that of orthorhombic $NaNbO_3$ [102]. Theoretical calculation show that a unique electronic structure and the presence of high symmetry in the cubic $NaNbO_3$ facilitates the charge excitation and separation process, which contributes to the enhanced photocatalytic activity, compared to the orthorhombic $NaNbO_3$ [102]. In addition, high crystalline $SrTiO_3$ (due to high synthesis temperature) showed enhanced photocatalytic activity because at high temperature, the number of defects, such as grain boundary (recombination site), decreases with the increase in calcination temperature [103]. High calcination temperature not only increases the crystallinity of the photocatalysts but also increases the particle size. High particle size can also lead to high H_2 evolution [103,104]. Moniruddin et al. [105] demonstrated that the crystallite size $SrTiO_3$ nanofibers have a strong influence on its photocatalytic activity. H_2 evolution tests were performed for different $SrTiO_3$ nanofibers crystallite sizes that were synthesized in two different conditions. Firstly, calcination temperatures were varied at a constant precursor concentration to synthesize a different crystallite size. The H_2 production rate increased with increasing calcination temperature and as well as increasing crystallite size. High calcination temperatures improve the crystallinity of $SrTiO_3$ and thus enhance H_2 evolution. Therefore, different $SrTiO_3$ nanofibers crystallite sizes were synthesized by changing the precursor concentrations at a constant calcination temperature to differentiate the crystallite size effect from crystallinity based on H_2 evolution. In both cases, the photocatalytic activity of $SrTiO_3$ nanofibers

increased with increasing crystallite size. Kim et al. [106] also demonstrated that nanoporous $BiVO_3$ significantly improved photoexcited charge separation and effectively suppressed the bulk carrier recombination when the crystal size become smaller than that of its hole diffusion length. Particle structure also influences the photocatalytic activity. For example, $SrTiO_3$ nanofibers exhibited two times higher photocatalytic activity than $SrTiO_3$ nanoparticles [105]. Here the particle-particle interconnection assembly builds up a well-ordered and aligned one-dimensional nanofiber that enhances photoexcited charge separation and assists with a faster interparticle charge transfer [107,108].

3.2.3. Plasmonic metal addition

The addition of plasmonic metal to the photocatalysts is another promising path to enhance charge separation and harnessing solar light in order to design efficient photocatalysts for water splitting [109,110]. Plasmonic materials show a collective oscillation of conduction electrons that oscillate at frequencies corresponding to light frequency, which can significantly alter the chemical and optical properties of a semiconductor while incorporating plasmonic materials [111,112]. Nanoparticles of Au and Ag have been widely used to improve visible light and generate surface plasmon resonance (SPR) hot electrons because of their high capability of promoting catalytic reactions. Xu et al. [34] demonstrated the effect of plasmonic Ag nanoparticles on the photocatalytic properties of $ATaO_3$ (A = Na, K) for water splitting. $ATaO_3$ (Na, K) without plasmonic metal does not show any photocatalytic activity under visible light, whereas Ag decorated $KTaO_3$ and $NaTaO_3$ nanocubes produced H_2. Lu et al. [113] recently designed an Au surface modified nanoporous single-crystalline SrTiO3 material to construct a plasmonic photocatalyst. The single-crystalline nature of $SrTiO_3$ enhances the mobility of SPR-induced photoelectrons, and its high surface area offers uniform dispersion of Au nanoparticles, which optimizes the diffusion region of SPR-induced photoelectrons than that of polycrystalline $SrTiO_3$. Therefore, embedding plasmonic metals on the perovskites provides another potential approach for developing new strategies in the design of water splitting photocatalysts.

3.2.4. Heterojunction formation

A suitable heterojunction nano-architecture, where electron-hole pairs are created in one semiconductor and afterward transported vectorially to adjacent materials, can absorb a wide range of the solar spectrum and efficiently separate the photoexcited electron-hole pairs [114,115]. $SrTiO_3$ and $NaTaO_3$ itself alone cannot split pure water, but after a heterostructure formation with NiO both photocatalysts can split pure water under UV irradiation [116,117]. However, the problem of capturing the visible light range remains. Therefore, different research groups were began focusing on the fabrication of heterojunction-based photocatalysts with both low and high band gap semiconductors to capture visible light and as well as to enhance charge separation and long-term stability. Low band gap semiconductors offer broad band light absorption, whereas many high band gap semiconductors are robust in an aqueous solution. Many $SrTiO_3$ composites, such as $SrTiO_3/Bi_2O_3$ [118], $SrTiO_3$/CdS [119], $SrTiO_3/MoS_2$ [120], and $SrTiO_3/Fe_2O_3$ [121], which exhibited higher visible light photocatalytic activity than that of pure $SrTiO_3$ for organic pollutant degradation, were fabricated. Recently, Wang et al. [122] investigated the geometry and electronic properties of $SrTiO_3/NaTaO_3$ heterostructures using hybrid density functional of HSE06. Their results suggested that $SrTiO_3/NaTaO_3$ heterostructures with six layers of $SrTiO_3$ and $NaTaO_3$ each have smaller band gaps (2.58 eV) as compared to those of pure $SrTiO_3$ and $NaTaO_3$, and they can be promising visible light photocatalysts for water splitting.

3.2.5. Utilizing ferroelectric materials polarization field

Ferroelectrics have currently attracted attention as a potential candidate for use in photocatalytic water splitting due to their spontaneous electric polarization, which promotes desirable photoexcited charge separation [123,124]. Some recent studies on a permanent electrical polarization field have shown some encouraging results in band engineering and the charge transport property at the interface of heterojunction-based photocatalysts. In a ferroelectric-based heterojunction, the electrical polarization of the ferroelectric material could redistribute the free carrier charge to the neighboring semiconductor and thus manipulating the depletion region's width and magnitude in a suitable direction [125]. A recent study by Yang et al. [126] demonstrated that introducing a ferroelectric perovskite material ($BaTiO_3$) in TiO_2/$BaTiO_3$ heterojunctions is a potential design strategy to improve photoelectrochemical cell performance. The spontaneous electrical polarization of $BaTiO_3$ film increased TiO_2 NWs band banding and improved the photoexcited charge separation, thus enhancing the photocurrent density of water oxidation reactions. Iyer et al. [127] also reported the ferroelectric effect of $BaTiO_3$ in $BaTiO_3/TiO_2$ heterojunctions using a density functional theory calculation. The direction of polarization (especially positive polarization) and thickness of the TiO_2 monolayer have positive impacts that enhance the oxygen evolution reaction (OER) performance. Lee et al. [128] showed that the $SrTiO_3$ polarization effect in the $SrTiO_3/TiO_2$ heterojunction in terms of OER activity using first-principles density functional theory calculations. $SrTiO_3/TiO_2$ heterojunction exhibited enhanced OER activity relative to pure TiO_2, due to the dynamical dipoles induced in response to the charge on the adsorbed species. However, ferroelectric materials have a high dielectric constant and are insulating in nature, which could be limiting factors in applying these materials to charge transport, especially in photocatalytic water splitting.

3.3. Recent progress of perovskite materials for water splitting

Perovskite materials as photocatalysts for water splitting have been actively explored because they have a suitable band gap position and have long term stability [94,129]. Titanate, tantalate and niobate perovskite are typically investigated in water splitting applications. Here, we mainly focused on $SrTiO_3$-based photocatalysts along with a brief update of other perovskite photocatalysts.

Most titanate perovskites show prominent photocatalytic activity under UV light. Among them, $SrTiO_3$ has been widely studied for hydrogen production as a photocatalyst for water splitting. Their photocatalytic activity can be extended towards the visible light range by doping suitable metal elements such as Ag, Cr, and Ta [130–132]. Cr-doped $SrTiO_3$, when loaded with Pt (0.6 wt%) nanoparticles as a cocatalyst, generates hydrogen of 82.6 μmol h^{-1} from a 20% aqueous methanol solution under visible light with an apparent quantum yield (AQY) of 2.95% [130]. Recently, Zhong et al. [133] used Au-NPs on the 0.05 wt% niobium-doped strontium titanate (Nb–$SrTiO_3$) single-crystal to develop a plasmon-induced water splitting system that operates under visible light. This system has two separate chambers for two different solution whereby hydrogen and oxygen gas are generated separately as shown in Fig. 8b. A localized surface plasmon resonance (LSPR) produced by the Au-NPs on the Nb–$SrTiO_3$ substrate facilitate the separation of charge at the Au/$SrTiO_3$ interface. This promotes the oxidation of water as well as the subsequent reduction of a proton on the backside of the same $SrTiO_3$ substrate. In the absence of Au-NPs, $SrTiO_3$ or Nb-doped, $SrTiO_3$ do not show any photocatalytic activity under visible light which demonstrate the plasmonic particles (Au) effect on this system. The efficiency of this system is dependent on the pH value of each chamber. The pH value in the H_2- and

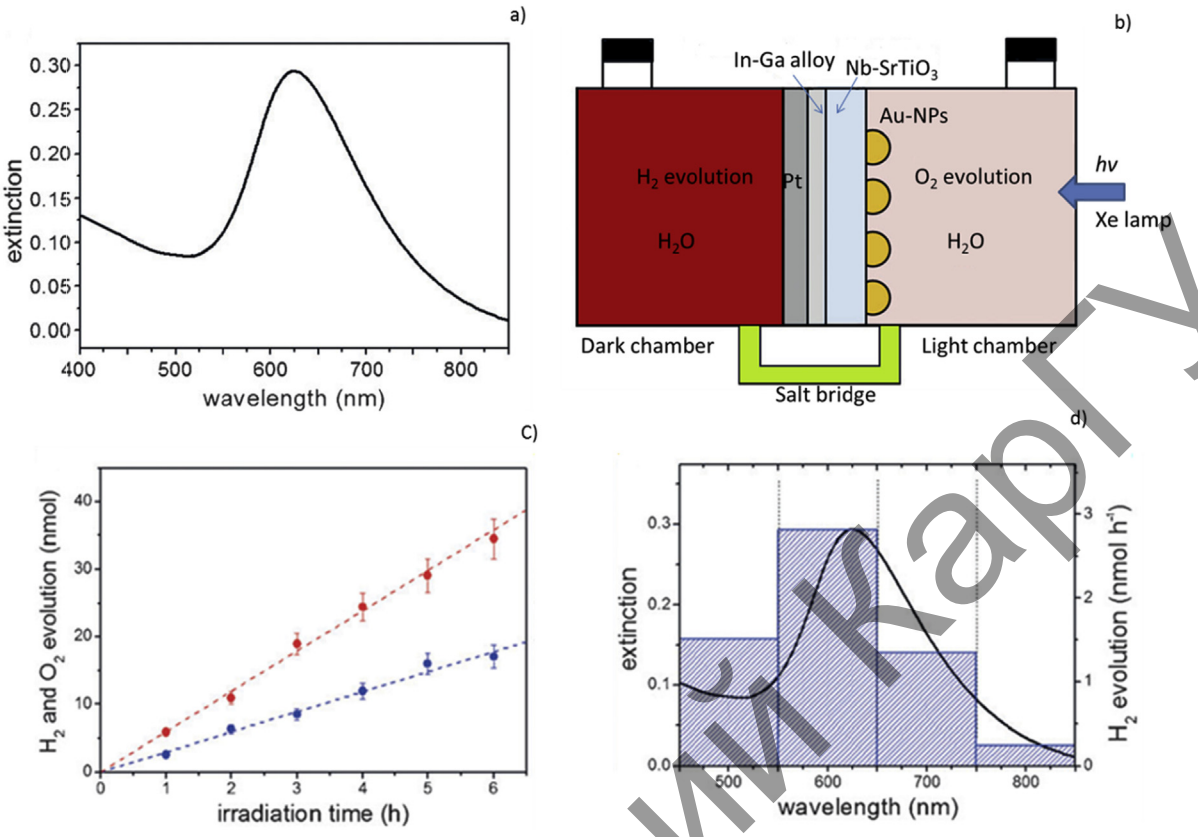

Fig. 8. (a) Extinction spectrum of Au-NPs on Nb–$SrTiO_3$. (b) schematic of the water splitting device; (c) time dependent H_2 (red circles) and O_2 (blue circles) evolution data in the back and front side chambers, respectively; and (d) H_2 evolution at different wavelength regions. (For interpretation of the references to colour in this figure legend, the reader is referred to the web version of this article.) Reprinted from Ref. [133].

O_2- evolution side are maintained at 1 and 13, respectively. It was found that the efficiency of both H_2 and O_2 gradually decreases with increases of pH on the H_2- evolution side, whereas at pH 4, the system does not exhibit any H_2 and O_2 production. The results of this system are given in Fig. 8. The heterojunction formation of $SrTiO_3$ with narrow band-gap semiconductors is another effective way to extend its light absorption range within the visible range and facilitate the photoinduced charge separation. Wu et al. [119] synthesized a $SrTiO_3$–CdS heterojunction which decontaminated hazardous wastewater containing antibiotics under visible light irradiation. Chang et al. [134] improved the photoinduced charge separation of $SrTiO_3$–CdS heterojunction by introducing Au at the interface between $SrTiO_3$ and CdS. The fabricated CdS/Au/3DOM-$SrTiO_3$ showed an enhanced hydrogen evolution rate of 5.46 mmol g^{-1} h^{-1} with AQE of 42.2% at a 420 nm wavelength light. Moreover, Cr-doped $SrTiO_3/TiO_2$ heterostructure nanotube arrays demonstrated higher photocatalytic performances than both pure TiO_2 nanotube arrays and $SrTiO_3/TiO_2$ nanotube arrays under visible light irradiation [135].

Kato et al. [136] utilized $SrTiO_3$ in Z-scheme system for overall water splitting, where two photocatalysts with appropriate band edge position complete the water redox reaction. In recent years, $SrTiO_3$ has been studied in the Z-scheme photocatalytic system due to its suitable CB position for hydrogen generation [91,137,138]. Sasaki et al. [139] investigated visible light driven Z-scheme systems composed of Ru/$SrTiO_3$:Rh as an H_2 evolving photocatalyst (HEP) and $BiVO_4$ as an O_2 evolving photocatalyst (OEP) in a suspended particle system to split water into H_2 and O_2. $[Co(bpy)_3]^{3+/2+}$ and $[Co(phen)_3]^{3+/2+}$ redox couples are used as an electron mediator in this system (Fig. 9a). This system is highly dependent on the pH of the aqueous medium and exhibits its highest activity under a neutral pH condition. Jia et al. [140] developed a $BiVO_4$–Ru/$SrTiO_3$:Rh composite Z-scheme system to eliminate the use of redox mediators. They prepared the $BiVO_4$–Ru/$SrTiO_3$:Rh composite using an impregnation method and a liquid–solid state reaction in which Ru/$SrTiO_3$:Rh particles act as an HEP and $BiVO_4$ particles as an OEP. In this composite, the electron is transferred directly through the interparticle interfacial area of $BiVO_4$ and Ru/$SrTiO_3$:Rh instead of any redox media (Fig. 9b). This system gives a AQY of 1.6% at 420 nm and shows stable activity. However, efficient electron transfer between the HEP and the OEP is one of the major hurdles to improve the efficiency of the composite Z-scheme water splitting system [141]. Recently, Wang et al. [142] developed an $SrTiO_3$:La,Rh/Au/$BiVO_4$:Mo composite sheet, whereby La- and Rh- codoped $SrTiO_3$ and Mo-doped $BiVO_4$ powders are embedded into a gold layer. It is believed that the support gold layer helps the electron transfer process between the HEP and OEP, which boosts up the performance of this Z-scheme. The system demonstrated an AQY of 30% at 419 nm and a solar to hydrogen (STH) energy conversion efficiency of 1.1% for overall water splitting, which is the highest reported AQY and STH among all other Z-scheme-based photocatalysts for suspended particle systems.

Tandem cell configuration is another well studied system for overall water splitting, which is similar to the Z-scheme [143–145]. Here, the solar cell provides the bias voltage to the photocatalysts to overcome the water splitting reaction energy barrier. When the organic-inorganic halide perovskite ($CH_3NH_3PbI_3$) solar cell is configured in tandem with a Fe_2O_3 photoanode, it exhibits a STH

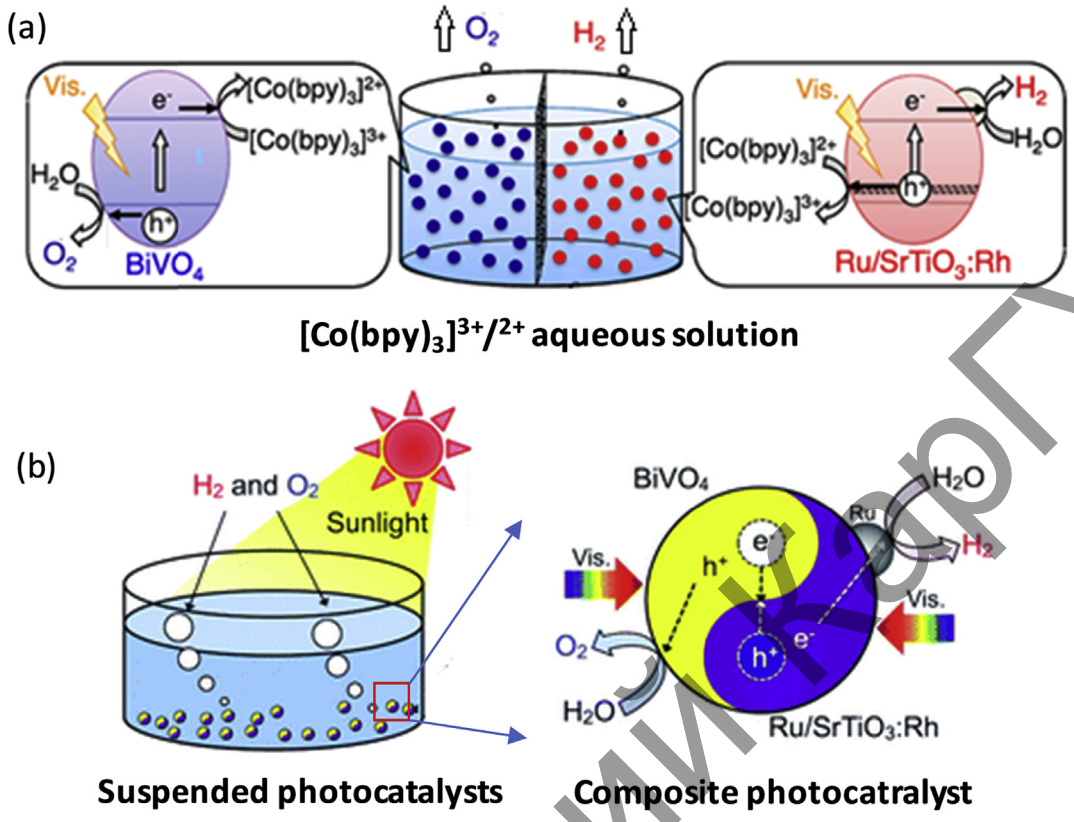

Fig. 9. Schematic of Z-scheme photocatalyst for overall water splitting system: (a) with redox mediator, and (b) without redox mediator. Reprinted from Ref. [139,140].

energy conversion efficiency of 2.4% for overall unassisted water splitting [146]. If the halide perovskite ($CH_3NH_3PbI_3$) solar cell is combined with the bifunctional NiFe layered double hydroxide electrode, it achieves high STH efficiency of 12.3% in an alkaline electrolyte [147]. However, in this configuration the cell lifetime is limited due to the degradation of the perovskite. An example of tandem cell configuration is shown in Fig. 10.

Some other PMs have been explored for their visible light photocatalytic activity. Recently, Park et al. [148] demonstrated H_2 production from hydrohalic acid (HX) using a halide perovskite named methylammonium lead iodide ($MAPbI_3$) under visible light irradiation. $MAPbI_3$ is not stable in water because it decomposes into the PbI_2 precipitate, methylammonium cation, and iodide anion. However, it is stable in an HI aqueous solution if added beyond its saturation limit. The precipitated $MAPbI_3$ powder could split HI into H_2 and I_3^- when irradiated with visible light (>475 nm). $NaTaO_3$ is an another well studied perovskite photocatalysts due to its tunable electronic and optical properties. Theoretical studies

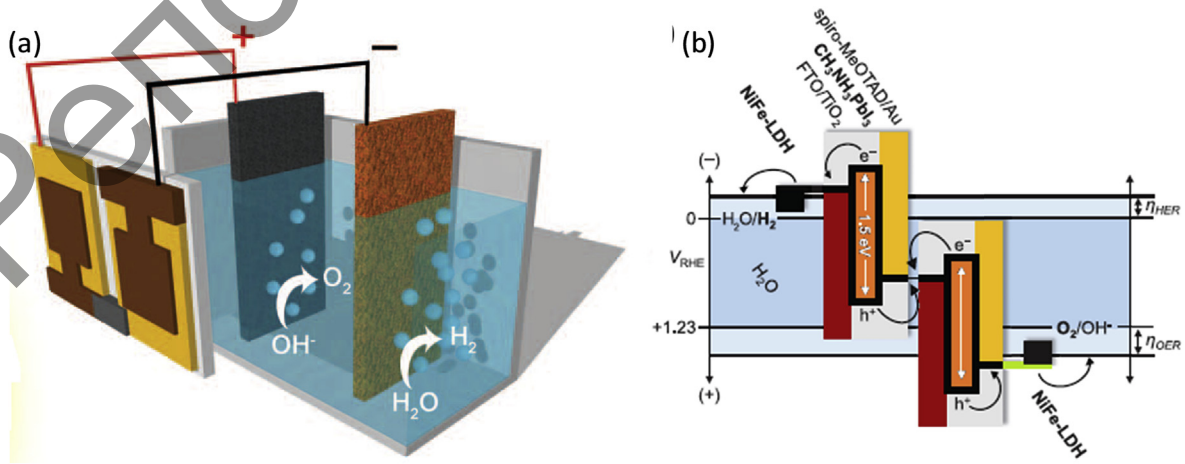

Fig. 10. (a) Schematic diagram of perovskite tandem cell with NiFe DLH/Ni foam electrodes for water-splitting device, and (b) energy schematic of perovskite tandem cell for water splitting. Reprinted from Ref. [147].

have shown that photocatalytic activity of $NaTaO_3$ can be extended to the visible light range by doping with carbon in the presence of Cr, Mo, or W and with nitrogen in presence of Mo [149,150]. Nitrogen-doped $NaTaO_3$-xN_x showed visible light photoactivity towards H_2 and O_2 generation from aqueous methanol and silver nitrate solutions, respectively [151]. $BiFeO_3$ can only generate oxygen under UV conditions [152], whereas $BiFeO_3$ nanoparticles coated with $SrTiO_3$ can produce H_2 under visible light irradiation [153]. Joshi et al. [154] demonstrated that $BiFeO_3$ nanocubes synthesized via a microwave technique can generate O_2 from an aqueous $FeCl_3$ solution. Moniz et al. [155] use dual-source low pressure chemical vapor deposition (LPCVD) to synthesize $BiFeO_3$ film, and with an Ni–B co-catalyst, this system exhibits considerable photocatalytic properties. Lu et al. [156] investigated a novel photocatalyst Ag/$BiFeO_3$, using the sol-gel process, which shows remarkable photocatalytic properties due to the surface plasmon resonance effect of Ag nanoparticles. Photocatalytic properties of other perovskite photocatalysts can be found in some recent review articles [91,124,157]. Pan et al. [158] developed a complex perovskite ($LaMgxTa_{1-x}O_{1+3x}N_{2-3x}$) that is able to do overall water splitting at wavelengths up to 600 nm. In this system, N_2 evolution was observed during the photoirradiation which suggests catalysts degradation due to the reaction between photoexcited holes (h^+) and nitrogen species at the catalysts surface. However, N_2 evolution can be minimized by applying an Si or Ti layer, thus preventing the catalyst degradation during photoirradiation.

4. Degradation

Perovskite materials are considered potential photocatalysts for both solar cell and water splitting due to their high photocatalytic activity and ease of synthesis. However, their stability is still a challenge in both PVs and water splitting application [84]. Electrical and chemical degradation are the most common phenomena for PMs during solar energy conversion. These degradations may depend on the irradiation time, temperature, pressure, moisture, and perovskite properties [159,160]. However, full insights into the degradation mechanism is still not clear. At high pressure, $MnTiO_3$ perovskite became unstable and decomposed into MnO and $MnTi_2O_5$ [161]. $ATiO_3$ (A = Zn, Fe) and $BiFeO_3$ were also known to decompose into two phases of AO and AB_2O_5 [162,163]. Though, Ti-doping can help to reduce the decomposition reaction of $BiFeO_3$ ceramics [162]. The dielectric properties of $BiFeO_3$ have been tested to demonstrate the decomposition of $BiFeO_3$, where dielectric loss is suppressed after Ti-doping [162]. Then, substantial degradation of catalytic activity occurred. Moreover, ferroelectric aging and resistance degradation typically influence photocatalytic activity of PMs [164–166]. A previous study on thermally stimulated relaxation in $SrTiO_3$:Fe showed that the resistance degradation involved trapped charge, defect dipoles, and oxygen vacancy motion [165]. Stefan et al. used micro contact impedance spectroscopy to determine the conductivity profiles of Fe doped strontium titanate perovskite. In this experiment, the blocking of grain boundaries and variations of oxygen-vacancies on the different sites of the grain boundaries are observed, which could be the possible explanation for the resistance degradation [167]. The time-dependent degradation of Y-doping SrTiO3 has been carried out by Ma et al. [168]. In this research, $Y_{0.07}Sr_{0.895}TiO_3$ was prepared, and impedance spectroscopy was used to examine the non-ohmic losses of this PSC. This system showed degradation after 500 h. Here, catalyst agglomeration and loss of electrical conductivity occurred synchronously with time [168]. More degradation phenomena on halide perovskite can be found in a recent review article ref. no 169 [169].

5. Summary and perspectives

Extensive research has only recently begun for the uses of perovskite solar cells and other optoelectronic applications; however, a great breakthrough in solar cells has been made utilizing organolead halide perovskites as sunlight absorbers with low-cost preparation techniques. Organolead halide perovskites are capable of harvesting a large amount of light, possess excellent electron transport properties, and have a low defect density and low intergrain potential barriers. Power conversion efficiencies of more than 15% have been reached for both mesoscopic architecture and planar heterojunction. Currently, it is believed that the major factors that can boost the performance of perovskite solar cells are increasing the crystals domain size and making a uniform perovskite film.

Some major progresses in the advancement of perovskite based photocatalysts for water splitting have also been accomplished by implementing different design strategies based on crystal structure and structural morphology, chemical component characteristics, heterojunction assembly, and the incorporation of plasmonic materials, ferroelectric materials, and different types of dopants to the PMs. However, the STH efficiency of any photocatalyst for overall water splitting is still very low (2%) [86]. Finding the right photocatalysts is still the major problem in overall water splitting. Individual photocatalysts provide some definite properties. Therefore, it is necessary to design a photocatalyst with multifunctionality that has a wide range of light harnessing capability, faster photoinduced charge separation ability, appropriate band edge position matching with water redox potential, and high catalytic active sites. Introducing a polarization field and high conductive material at the heterojunction interface to improve the photoinduced charge separation could be an effective direction towards improving the efficiency of photocatalysts. The heterostructure formation with a low and high band gap semiconductor and designing surface morphology could improve the light harnessing capability. Stability of the low band gap semiconductors is one of the major issues. More research studies should be conducted to prevent photocorrosion in an aqueous solution, though, some studies have shown promise to prevent photocorrosion by using a TiO_2 coating and graphene layer [170,171].

Acknowledgment

This work was supported by ACS PRF. Authors gratefully acknowledges Texas Tech University for the support of this work.

References

[1] A.J. Nozik, Photoelectrochemistry: applications to solar energy conversion, Annu. Rev. Phys. Chem. 29 (1978) 189–222.
[2] N.S. Lewis, Powering the planet, MRS Bull. 32 (2007) 808–820.
[3] D.G. Nocera, Personalized energy: the home as a solar power station and solar gas station, ChemSusChem 2 (2009) 387–390.
[4] H. Wei, D. Cui, J. Ma, L. Chu, X. Zhao, H. Song, H. Liu, T. Liu, N. Wang, Z. Guo, Energy conversion technologies towards self-powered electrochemical energy storage systems: the state of the art and perspectives, J. Mater. Chem. A 5 (2017) 1873–1894.
[5] M. Moniruddin, B. Ilyassov, E. Seliverstova, Y. Shabdan, N. Bakranov, N. Ibrayev, N. Nuraje, Bioinspired study of energy and electron transfer in photovoltaic system, J. Exp. Nanosci. (2017) 1–12.
[6] Y. Shabdan, A. Ronasi, P. Coulibaly, M. Moniruddin, N. Nuraje, Engineered core-shell nanofibers for electron transport study in dye-sensitized solar cells, AIP Adv. 7 (2017) 065008.
[7] S.Z. Islam, A. Reed, D.Y. Kim, S.E. Rankin, N2/Ar plasma induced doping of ordered mesoporous TiO2 thin films for visible light active photocatalysis, Microporous Mesoporous Mater. 220 (2016) 120–128.
[8] S. De Wolf, J. Holovsky, S.-J. Moon, P. Löper, B. Niesen, M. Ledinsky, F.-J. Haug, J.-H. Yum, C. Ballif, Organometallic halide perovskites: sharp optical absorption edge and its relation to photovoltaic performance, J. Phys. Chem. Lett. 5 (2014) 1035–1039.

[9] A. Sadhanala, F. Deschler, T.H. Thomas, S.E. Dutton, K.C. Goedel, F.C. Hanusch, M.L. Lai, U. Steiner, T. Bein, P. Docampo, Preparation of single-phase films of CH3NH3Pb (I1−x Br x) 3 with sharp optical band edges, J. Phys. Chem. Lett. 5 (2014) 2501−2505.

[10] S.D. Stranks, G.E. Eperon, G. Grancini, C. Menelaou, M.J. Alcocer, T. Leijtens, L.M. Herz, A. Petrozza, H.J. Snaith, Electron-hole diffusion lengths exceeding 1 micrometer in an organometal trihalide perovskite absorber, Science 342 (2013) 341−344.

[11] G. Xing, N. Mathews, S. Sun, S.S. Lim, Y.M. Lam, M. Grätzel, S. Mhaisalkar, T.C. Sum, Long-range balanced electron-and hole-transport lengths in organic-inorganic $CH_3NH_3PbI_3$, Science 342 (2013) 344−347.

[12] V. Gonzalez-Pedro, E.J. Juarez-Perez, W.-S. Arsyad, E.M. Barea, F. Fabregat-Santiago, I. Mora-Sero, J. Bisquert, General working principles of CH3NH3PbX3 perovskite solar cells, Nano Lett. 14 (2014) 888−893.

[13] C. Wehrenfennig, G.E. Eperon, M.B. Johnston, H.J. Snaith, L.M. Herz, High charge carrier mobilities and lifetimes in organolead trihalide perovskites, Adv. Mater. 26 (2014) 1584−1589.

[14] E. Edri, S. Kirmayer, S. Mukhopadhyay, K. Gartsman, G. Hodes, D. Cahen, Elucidating the charge carrier separation and working mechanism of $CH_3NH_3PbI_3-$ xClx perovskite solar cells, Nat. Commun. 5 (2014) 3461.

[15] T. Liu, L. Yu, H. Liu, Q. Hou, C. Wang, H. He, J. Li, N. Wang, J. Wang, Z. Guo, Ni nanobelts induced enhancement of hole transport and collection for high efficiency and ambient stable mesoscopic perovskite solar cells, J. Mater. Chem. A 5 (2017) 4292−4299.

[16] T. Liu, C. Wang, J. Hou, C. Zhang, H. Chen, H. He, N. Wang, H. Wu, G. Cao, Enhanced electron collection in perovskite solar cells employing thermo-electric $NaCo_2O_4/TiO_2$ coaxial nanofibers, Small 12 (2016) 5146−5152.

[17] W. Hu, T. Liu, X. Yin, H. Liu, X. Zhao, S. Luo, Y. Guo, Z. Yao, J. Wang, N. Wang, Hematite electron-transporting layers for environmentally stable planar perovskite solar cells with enhanced energy conversion and lower hysteresis, J. Mater. Chem. A 5 (2017) 1434−1441.

[18] Y. Guo, T. Liu, N. Wang, Q. Luo, H. Lin, J. Li, Q. Jiang, L. Wu, Z. Guo, Ni-doped α-Fe_2O_3 as electron transporting material for planar heterojunction perovskite solar cells with improved efficiency, reduced hysteresis and ultraviolet stability, Nano Energy 38 (2017) 193−200.

[19] M.M. Lee, J. Teuscher, T. Miyasaka, T.N. Murakami, H.J. Snaith, Efficient hybrid solar cells based on meso-superstructured organometal halide perovskites, Science 338 (2012) 643−647.

[20] H. Zhou, Q. Chen, G. Li, S. Luo, T.-B. Song, H.-S. Duan, Z. Hong, J. You, Y. Liu, Y. Yang, Interface engineering of highly efficient perovskite solar cells, Science 345 (2014) 542−546.

[21] H.-S. Kim, C.-R. Lee, J.-H. Im, K.-B. Lee, T. Moehl, A. Marchioro, S.-J. Moon, R. Humphry-Baker, J.-H. Yum, J.E. Moser, Lead iodide perovskite sensitized all-solid-state submicron thin film mesoscopic solar cell with efficiency exceeding 9%, Sci. Rep. 2 (2012).

[22] W.S. Yang, B.-W. Park, E.H. Jung, N.J. Jeon, Y.C. Kim, D.U. Lee, S.S. Shin, J. Seo, E.K. Kim, J.H. Noh, Iodide management in formamidinium-lead-halide−based perovskite layers for efficient solar cells, Science 356 (2017) 1376−1379.

[23] M.A. Green, K. Emery, Y. Hishikawa, W. Warta, E.D. Dunlop, Solar cell efficiency tables (Version 45), Prog. Photovolt. Res. Appl. 23 (2015) 1−9.

[24] M. Ni, M.K. Leung, D.Y. Leung, K. Sumathy, A review and recent developments in photocatalytic water-splitting using TiO_2 for hydrogen production, Renew. Sustain. Energy Rev. 11 (2007) 401−425.

[25] M. Moniruddin, S. Kudaibergenov, N. Nuraje, Chapter 7 hierarchical nano-heterostructures for water splitting, in: Green Photo-active Nanomaterials: Sustainable Energy and Environmental Remediation, The Royal Society of Chemistry, 2016, pp. 142−167.

[26] C. Burda, Y. Lou, X. Chen, A.C. Samia, J. Stout, J.L. Gole, Enhanced nitrogen doping in TiO2 nanoparticles, Nano Lett. 3 (2003) 1049−1051.

[27] S.Z. Islam, A. Reed, N. Wanninayake, D.Y. Kim, S.E. Rankin, Remarkable enhancement of photocatalytic water oxidation in N2/Ar plasma treated, mesoporous TiO2 films, J. Phys. Chem. C 120 (2016) 14069−14081.

[28] J.H. Park, S. Kim, A.J. Bard, Novel carbon-doped TiO2 nanotube arrays with high aspect ratios for efficient solar water splitting, Nano Lett. 6 (2006) 24−28.

[29] N. Nuraje, Y. Lei, A. Belcher, Virus-templated visible spectrum active perovskite photocatalyst, Catal. Commun. 44 (2014) 68−72.

[30] H. Kato, A. Kudo, Water splitting into H2 and O2 on alkali tantalate photocatalysts ATaO3 (A= Li, Na, and K), J. Phys. Chem. B 105 (2001) 4285−4292.

[31] A. Kudo, Y. Miseki, Heterogeneous photocatalyst materials for water splitting, Chem. Soc. Rev. 38 (2009) 253−278.

[32] D. Damjanovic, Piezoelectric properties of perovskite ferroelectrics: unsolved problems and future research, in: Annales de Chimie Science des Materiaux, Elsevier, 2001, pp. 99−106.

[33] N. Nuraje, K. Su, Perovskite ferroelectric nanomaterials, Nanoscale 5 (2013) 8752−8780.

[34] D. Xu, S. Yang, Y. Jin, M. Chen, W. Fan, B. Luo, W. Shi, Ag-decorated ATaO3 (A= K, Na) nanocube plasmonic photocatalysts with enhanced photocatalytic water-splitting properties, Langmuir 31 (2015) 9694−9699.

[35] A. Iwase, H. Kato, A. Kudo, Nanosized Au particles as an efficient cocatalyst for photocatalytic overall water splitting, Catal. Lett. 108 (2006) 7−10.

[36] E. Knittle, R. Jeanloz, Synthesis and equation of state of (Mg, Fe) SiO3 perovskite to over 100 gigapascals, Science 235 (1987) 668−671.

[37] Z. Cheng, J. Lin, Layered organic−inorganic hybrid perovskites: structure, optical properties, film preparation, patterning and templating engineering, CrystEngComm 12 (2010) 2646−2662.

[38] A. Glazer, The classification of tilted octahedra in perovskites, Acta Crystallogr. Sect. B Struct. Crystallogr. Cryst. Chem. 28 (1972) 3384−3392.

[39] D.E. Scaife, P.F. Weller, W.G. Fisher, Crystal preparation and properties of cesium tin (II) trihalides, J. Solid State Chem. 9 (1974) 308−314.

[40] N.-G. Park, Crystal growth engineering for high efficiency perovskite solar cells, Cryst. Eng. Comm. 18 (2016) 5977−5985.

[41] M.A. Green, A. Ho-Baillie, H.J. Snaith, The emergence of perovskite solar cells, Nat. Photonics 8 (2014) 506−514.

[42] P. Umari, E. Mosconi, F. De Angelis, Relativistic GW calculations on $CH_3NH_3PbI_3$ and $CH_3NH_3SnI_3$ perovskites for solar cell applications, Sci. Rep. 4 (2014) 4467.

[43] R. Coontz, Science's Top 10 Breakthroughs of 2013, 2013.

[44] T. Liu, J. Hou, B. Wang, F. Bai, H. Chen, L. Gao, Y. Cao, H. He, J. Wang, N. Wang, Correlation between the in-plain substrate strain and electrocatalytic activity of strontium ruthenate thin films in dye-sensitized solar cells, J. Mater. Chem. A 4 (2016) 10794−10800.

[45] H. He, C. Zhang, T. Liu, Y. Cao, N. Wang, Z. Guo, Thermoelectric−photoelectric composite nanocables induced a larger efficiency in dye-sensitized solar cells, J. Mater. Chem. A 4 (2016) 9362−9369.

[46] A. Kojima, K. Teshima, Y. Shirai, T. Miyasaka, Organometal halide perovskites as visible-light sensitizers for photovoltaic cells, J. Am. Chem. Soc. 131 (2009) 6050−6051.

[47] V. D'innocenzo, G. Grancini, M.J. Alcocer, A.R.S. Kandada, S.D. Stranks, M.M. Lee, G. Lanzani, H.J. Snaith, A. Petrozza, Excitons versus free charges in organo-lead tri-halide perovskites, Nat. Commun. 5 (2014) 3586.

[48] J.H. Heo, S.H. Im, J.H. Noh, T.N. Mandal, C.-S. Lim, J.A. Chang, Y.H. Lee, H.-J. Kim, A. Sarkar, M.K. Nazeeruddin, Efficient inorganic-organic hybrid heterojunction solar cells containing perovskite compound and polymeric hole conductors, Nat. Photonics 7 (2013) 486−491.

[49] J. Burschka, N. Pellet, S.-J. Moon, R. Humphry-Baker, P. Gao, M.K. Nazeeruddin, M. Grätzel, Sequential deposition as a route to high-performance perovskite-sensitized solar cells, Nature 499 (2013) 316.

[50] M. Liu, M.B. Johnston, H.J. Snaith, Efficient planar heterojunction perovskite solar cells by vapour deposition, Nature 501 (2013) 395.

[51] Perovskite Solar Cells, 2017.

[52] J.M. Ball, M.M. Lee, A. Hey, H.J. Snaith, Low-temperature processed meso-superstructured to thin-film perovskite solar cells, Energy Environ. Sci. 6 (2013) 1739−1743.

[53] G.E. Eperon, V.M. Burlakov, P. Docampo, A. Goriely, H.J. Snaith, Morphological control for high performance, solution-processed planar heterojunction perovskite solar cells, Adv. Funct. Mater. 24 (2014) 151−157.

[54] S. Sun, T. Salim, N. Mathews, M. Duchamp, C. Boothroyd, G. Xing, T.C. Sum, Y.M. Lam, The origin of high efficiency in low-temperature solution-processable bilayer organometal halide hybrid solar cells, Energy Environ. Sci. 7 (2014) 399−407.

[55] J.Y. Jeng, Y.F. Chiang, M.H. Lee, S.R. Peng, T.F. Guo, P. Chen, T.C. Wen, $CH_3NH_3PbI_3$ perovskite/fullerene planar-heterojunction hybrid solar cells, Adv. Mater. 25 (2013) 3727−3732.

[56] S. Dharani, H.K. Mulmudi, N. Yantara, P.T.T. Trang, N.G. Park, M. Graetzel, S. Mhaisalkar, N. Mathews, P.P. Boix, High efficiency electrospun TiO 2 nanofiber based hybrid organic−inorganic perovskite solar cell, Nanoscale 6 (2014) 1675−1679.

[57] K. Liang, D.B. Mitzi, M.T. Prikas, Synthesis and characterization of organic−inorganic perovskite thin films prepared using a versatile two-step dipping technique, Chem. Mater. 10 (1998) 403−411.

[58] Q. Chen, H. Zhou, Z. Hong, S. Luo, H.-S. Duan, H.-H. Wang, Y. Liu, G. Li, Y. Yang, Planar heterojunction perovskite solar cells via vapor-assisted solution process, J. Am. Chem. Soc. 136 (2013) 622−625.

[59] O. Malinkiewicz, A. Yella, Y.H. Lee, G.M. Espallargas, M. Graetzel, M.K. Nazeeruddin, H.J. Bolink, Perovskite solar cells employing organic charge-transport layers, Nat. Photonics 8 (2014) 128−132.

[60] H.J. Snaith, L. Schmidt-Mende, Advances in liquid-electrolyte and solid-state dye-sensitized solar cells, Adv. Mater. 19 (2007) 3187−3200.

[61] D. Liu, T.L. Kelly, Perovskite solar cells with a planar heterojunction structure prepared using room-temperature solution processing techniques, Nat. Photonics 8 (2014) 133−138.

[62] E. Edri, S. Kirmayer, A. Henning, S. Mukhopadhyay, K. Gartsman, Y. Rosenwaks, G. Hodes, D. Cahen, Why lead methylammonium tri-iodide perovskite-based solar cells require a mesoporous electron transporting scaffold (but not necessarily a hole conductor), Nano Lett. 14 (2014) 1000−1004.

[63] B. Conings, L. Baeten, C. De Dobbelaere, J. D'Haen, J. Manca, H.G. Boyen, Perovskite-based hybrid solar cells exceeding 10% efficiency with high reproducibility using a thin film sandwich approach, Adv. Mater. 26 (2014) 2041−2046.

[64] D.B. Mitzi, K. Chondroudis, C.R. Kagan, Organic-inorganic electronics, IBM J. Res. Dev. 45 (2001) 29−45.

[65] P. Docampo, J.M. Ball, M. Darwich, G.E. Eperon, H.J. Snaith, Efficient organometal trihalide perovskite planar-heterojunction solar cells on flexible polymer substrates, Nat. Commun. 4 (2013).

[66] G.E. Eperon, V.M. Burlakov, A. Goriely, H.J. Snaith, Neutral color semitransparent microstructured perovskite solar cells, ACS Nano 8 (2013) 591–598.

[67] H.S. Jung, N.G. Park, Perovskite solar cells: from materials to devices, Small 11 (2015) 10–25.

[68] J. Even, L. Pedesseau, C. Katan, Analysis of multivalley and multibandgap absorption and enhancement of free carriers related to exciton screening in hybrid perovskites, J. Phys. Chem. C 118 (2014) 11566–11572.

[69] M. Saba, M. Cadelano, D. Marongiu, F. Chen, V. Sarritzu, N. Sestu, C. Figus, M. Aresti, R. Piras, A.G. Lehmann, Correlated electron-hole plasma in organometal perovskites, Nat. Commun. 5 (2014) 5049.

[70] S.D. Stranks, V.M. Burlakov, T. Leijtens, J.M. Ball, A. Goriely, H.J. Snaith, Recombination kinetics in organic-inorganic perovskites: excitons, free charge, and subgap states, Phys. Rev. Appl. 2 (2014) 034007.

[71] F. Deschler, M. Price, S. Pathak, L.E. Klintberg, D.-D. Jarausch, R. Higler, S. Hüttner, T. Leijtens, S.D. Stranks, H.J. Snaith, High photoluminescence efficiency and optically pumped lasing in solution-processed mixed halide perovskite semiconductors, J. Phys. Chem. Lett. 5 (2014) 1421–1426.

[72] C.S. Ponseca Jr., T.J. Savenije, M. Abdellah, K. Zheng, A. Yartsev, T.R. Pascher, T. Harlang, P. Chabera, T. Pullerits, A. Stepanov, Organometal halide perovskite solar cell materials rationalized: ultrafast charge generation, high and microsecond-long balanced mobilities, and slow recombination, J. Am. Chem. Soc. 136 (2014) 5189–5192.

[73] T. Leijtens, S.D. Stranks, G.E. Eperon, R. Lindblad, E.M. Johansson, I.J. McPherson, H. Rensmo, J.M. Ball, M.M. Lee, H.J. Snaith, Electronic properties of meso-superstructured and planar organometal halide perovskite films: charge trapping, photodoping, and carrier mobility, ACS Nano 8 (2014) 7147–7155.

[74] J.S. Manser, P.V. Kamat, Band filling with free charge carriers in organometal halide perovskites, Nat. Photonics 8 (2014) 737–743.

[75] K. Tvingstedt, O. Malinkiewicz, A. Baumann, C. Deibel, H.J. Snaith, V. Dyakonov, H.J. Bolink, Radiative efficiency of lead iodide based perovskite solar cells, Sci. Rep. 4 (2014).

[76] O.D. Miller, E. Yablonovitch, S.R. Kurtz, Strong internal and external luminescence as solar cells approach the Shockley–Queisser limit, IEEE J. Photovolt. 2 (2012) 303–311.

[77] W. Tress, N. Marinova, O. Inganäs, M. Nazeeruddin, S.M. Zakeeruddin, M. Graetzel, Predicting the open-circuit voltage of $CH_3NH_3PbI_3$ perovskite solar cells using electroluminescence and photovoltaic quantum efficiency spectra: the role of radiative and non-radiative recombination, Adv. Energy Mater. 5 (2015).

[78] Y. Shao, Z. Xiao, C. Bi, Y. Yuan, J. Huang, Origin and elimination of photocurrent hysteresis by fullerene passivation in $CH_3NH_3PbI_3$ planar heterojunction solar cells, Nat. Commun. 5 (2014) 5784.

[79] Q. Dong, Y. Fang, Y. Shao, P. Mulligan, J. Qiu, L. Cao, J. Huang, Electron-hole diffusion lengths >175 μm in solution-grown $CH_3NH_3PbI_3$ single crystals, Science 347 (2015) 967–970.

[80] D. Shi, V. Adinolfi, R. Comin, M. Yuan, E. Alarousu, A. Buin, Y. Chen, S. Hoogland, A. Rothenberger, K. Katsiev, Low trap-state density and long carrier diffusion in organolead trihalide perovskite single crystals, Science 347 (2015) 519–522.

[81] T. Leijtens, B. Lauber, G.E. Eperon, S.D. Stranks, H.J. Snaith, The importance of perovskite pore filling in organometal mixed halide sensitized TiO_2-based solar cells, J. Phys. Chem. Lett. 5 (2014) 1096–1102.

[82] N.J. Jeon, J.H. Noh, Y.C. Kim, W.S. Yang, S. Ryu, S.I. Seok, Solvent engineering for high-performance inorganic–organic hybrid perovskite solar cells, Nat. Mater. 13 (2014) 897–903.

[83] N.J. Jeon, J.H. Noh, W.S. Yang, Y.C. Kim, S. Ryu, J. Seo, S.I. Seok, Compositional engineering of perovskite materials for high-performance solar cells, Nature 517 (2015) 476.

[84] H.J. Snaith, Perovskites: the emergence of a new era for low-cost, high-efficiency solar cells, J. Phys. Chem. Lett. 4 (2013) 3623–3630.

[85] G. Zhang, Z.-A. Lan, L. Lin, S. Lin, X. Wang, Overall water splitting by Pt/gC 3 N 4 photocatalysts without using sacrificial agents, Chem. Sci. 7 (2016) 3062–3066.

[86] J. Liu, Y. Liu, N. Liu, Y. Han, X. Zhang, H. Huang, Y. Lifshitz, S.-T. Lee, J. Zhong, Z. Kang, Metal-free efficient photocatalyst for stable visible water splitting via a two-electron pathway, Science 347 (2015) 970–974.

[87] A. Tanaka, K. Teramura, S. Hosokawa, H. Kominami, T. Tanaka, Visible light-induced water splitting in an aqueous suspension of a plasmonic Au/TiO 2 photocatalyst with metal co-catalysts, Chem. Sci. 8 (2017) 2574–2580.

[88] D. Jiang, Z. Sun, H. Jia, D. Lu, P. Du, A cocatalyst-free CdS nanorod/ZnS nanoparticle composite for high-performance visible-light-driven hydrogen production from water, J. Mater. Chem. A 4 (2016) 675–683.

[89] L. Zhang, W. Yu, C. Han, J. Guo, Q. Zhang, H. Xie, Q. Shao, Z. Sun, Z. Guo, Large scaled synthesis of heterostructured electrospun TiO_2/SnO_2 nanofibers with an enhanced photocatalytic activity, J. Electrochem. Soc. 164 (2017) H651–H656.

[90] P. Xiao, W. Chen, X. Wang, A review of phosphide-based materials for electrocatalytic hydrogen evolution, Adv. Energy Mater. 5 (2015).

[91] P. Kanhere, Z. Chen, A review on visible light active perovskite-based photocatalysts, Molecules 19 (2014) 19995–20022.

[92] K. Maeda, K. Domen, New non-oxide photocatalysts designed for overall water splitting under visible light, J. Phys. Chem. C 111 (2007) 7851–7861.

[93] R.M. Navarro Yerga, M.C. Álvarez Galván, F. Del Valle, J.A. Villoria de la Mano, J.L. Fierro, Water splitting on semiconductor catalysts under visible-light irradiation, ChemSusChem 2 (2009) 471–485.

[94] N. Nuraje, R. Asmatulu, S. Kudaibergenov, Metal oxide-based functional materials for solar energy conversion: a review, Curr. Inorg. Chem. 2 (2012) 124–146.

[95] R. Konta, T. Ishii, H. Kato, A. Kudo, Photocatalytic activities of noble metal ion doped $SrTiO_3$ under visible light irradiation, J. Phys. Chem. B 108 (2004) 8992–8995.

[96] T. Ohno, T. Tsubota, Y. Nakamura, K. Sayama, Preparation of S, C cation-codoped $SrTiO_3$ and its photocatalytic activity under visible light, Appl. Catal. A Gen. 288 (2005) 74–79.

[97] K. Iwashina, A. Kudo, Rh-doped $SrTiO_3$ photocatalyst electrode showing cathodic photocurrent for water splitting under visible-light irradiation, J. Am. Chem. Soc. 133 (2011) 13272–13275.

[98] J.-P. Zou, L.-Z. Zhang, S.-L. Luo, L.-H. Leng, X.-B. Luo, M.-J. Zhang, Y. Luo, G.-C. Guo, Preparation and photocatalytic activities of two new Zn-doped SrTiO 3 and BaTiO 3 photocatalysts for hydrogen production from water without cocatalysts loading, Int. J. Hydrogen Energy 37 (2012) 17068–17077.

[99] W. Wang, M.O. Tadé, Z. Shao, Research progress of perovskite materials in photocatalysis-and photovoltaics-related energy conversion and environmental treatment, Chem. Soc. Rev. 44 (2015) 5371–5408.

[100] B. Wang, P.D. Kanhere, Z. Chen, J. Nisar, B. Pathak, R. Ahuja, Anion-doped $NaTaO_3$ for visible light photocatalysis, J. Phys. Chem. C 117 (2013) 22518–22524.

[101] F.-F. Li, D.-R. Liu, G.-M. Gao, B. Xue, Y.-S. Jiang, Improved visible-light photocatalytic activity of NaTaO 3 with perovskite-like structure via sulfur anion doping, Appl. Catal. B Environ. 166 (2015) 104–111.

[102] P. Li, S. Ouyang, G. Xi, T. Kako, J. Ye, The effects of crystal structure and electronic structure on photocatalytic H_2 evolution and CO_2 reduction over two phases of perovskite-structured $NaNbO_3$, J. Phys. Chem. C 116 (2012) 7621–7628.

[103] A. Kudo, A. Tanaka, K. Domen, T. Onishi, The effects of the calcination temperature of $SrTiO_3$ powder on photocatalytic activities, J. Catal. 111 (1988) 296–301.

[104] L. Macaraig, S. Chuangchote, T. Sagawa, Electrospun $SrTiO_3$ nanofibers for photocatalytic hydrogen generation, J. Mater. Res. 29 (2014) 123–130.

[105] M. Moniruddin, K. Afroz, Y. Shabdan, B. Bizri, N. Nuraje, Hierarchically 3D assembled strontium titanate nanomaterials for water splitting application, Appl. Surf. Sci. 419 (2017) 886–892.

[106] T.W. Kim, K.-S. Choi, Nanoporous $BiVO_4$ photoanodes with dual-layer oxygen evolution catalysts for solar water splitting, Science 343 (2014) 990–994.

[107] H. Bai, Z. Liu, D.D. Sun, Facile fabrication of $TiO_2/SrTiO_3$ composite nanofibers by electrospinning for high efficient H_2 generation, J. Am. Ceram. Soc. 96 (2013) 942–949.

[108] S.K. Choi, S. Kim, S.K. Lim, H. Park, Photocatalytic comparison of TiO_2 nanoparticles and electrospun TiO_2 nanofibers: effects of mesoporosity and interparticle charge transfer, J. Phys. Chem. C 114 (2010) 16475–16480.

[109] C. Clavero, Plasmon-induced hot-electron generation at nanoparticle/metal-oxide interfaces for photovoltaic and photocatalytic devices, Nat. Photonics 8 (2014) 95–103.

[110] J. Zhang, X. Jin, P.I. Morales-Guzman, X. Yu, H. Liu, H. Zhang, L. Razzari, J.P. Claverie, Engineering the absorption and field enhancement properties of Au–TiO_2 nanohybrids via whispering gallery mode resonances for photocatalytic water splitting, ACS Nano 10 (2016) 4496–4503.

[111] J. Lee, S. Mubeen, X. Ji, G.D. Stucky, M. Moskovits, Plasmonic photoanodes for solar water splitting with visible light, Nano Lett. 12 (2012) 5014–5019.

[112] S.C. Warren, E. Thimsen, Plasmonic solar water splitting, Energy Environ. Sci. 5 (2012) 5133–5146.

[113] D. Lu, S. Ouyang, H. Xu, D. Li, X. Zhang, Y. Li, J. Ye, Designing Au surface-modified nanoporous-single-crystalline $SrTiO_3$ to optimize diffusion of surface plasmon resonance-induce photoelectron toward enhanced visible-light photoactivity, ACS Appl. Mater. Interfaces 8 (2016) 9506–9513.

[114] J. Su, L. Guo, N. Bao, C.A. Grimes, Nanostructured $WO_3/BiVO_4$ heterojunction films for efficient photoelectrochemical water splitting, Nano Lett. 11 (2011) 1928–1933.

[115] D.J. Martin, P.J.T. Reardon, S.J.A. Moniz, J. Tang, Visible light-driven pure water splitting by a nature-inspired organic semiconductor-based system, J. Am. Chem. Soc. 136 (2014) 12568–12571.

[116] T.K. Townsend, N.D. Browning, F.E. Osterloh, Nanoscale strontium titanate photocatalysts for overall water splitting, ACS Nano 6 (2012) 7420–7426.

[117] T. Yokoi, J. Sakuma, K. Maeda, K. Domen, T. Tatsumi, J.N. Kondo, Preparation of a colloidal array of $NaTaO_3$ nanoparticles via a confined space synthesis route and its photocatalytic application, Phys. Chem. Chem. Phys. 13 (2011) 2563–2570.

[118] H. Che, J. Chen, K. Huang, W. Hu, H. Hu, X. Liu, G. Che, C. Liu, W. Shi, Construction of $SrTiO_3/Bi_2O_3$ heterojunction towards to improved separation efficiency of charge carriers and photocatalytic activity under visible light, J. Alloys Compd. 688 (2016) 882–890.

[119] G. Wu, L. Xiao, W. Gu, W. Shi, D. Jiang, C. Liu, Fabrication and excellent visible-light-driven photodegradation activity for antibiotics of $SrTiO_3$ nanocube coated CdS microsphere heterojunctions, RSC Adv. 6 (2016) 19878–19886.

[120] J. Liu, L. Zhang, N. Li, Q. Tian, J. Zhou, Y. Sun, Synthesis of MoS 2/$SrTiO_3$ composite materials for enhanced photocatalytic activity under UV irradiation, J. Mater. Chem. A 3 (2015) 706–712.

[121] C. Liu, G. Wu, J. Chen, K. Huang, W. Shi, Fabrication of a visible-light-driven photocatalyst and degradation of tetracycline based on the photoinduced interfacial charge transfer of $SrTiO_3/Fe_2O_3$ nanowires, New J. Chem. 40 (2016) 5198–5208.

[122] G.Z. Wang, H. Chen, X.K. Luo, H.K. Yuan, A.L. Kuang, Bandgap engineering of SrTiO3/NaTaO3 heterojunction for visible light photocatalysis, Int. J. Quantum Chem. 117 (2017) e25424-n/a.

[123] S.M. Young, A.M. Rappe, First principles calculation of the shift current photovoltaic effect in ferroelectrics, Phys. Rev. Lett. 109 (2012) 116601.

[124] I. Grinberg, D.V. West, M. Torres, G. Gou, D.M. Stein, L. Wu, G. Chen, E.M. Gallo, A.R. Akbashev, P.K. Davies, Perovskite oxides for visible-light-absorbing ferroelectric and photovoltaic materials, Nature 503 (2013) 509.

[125] J. Shi, P. Zhao, X. Wang, Piezoelectric-polarization-enhanced photovoltaic performance in depleted-heterojunction quantum-dot solar cells, Adv. Mater. 25 (2013) 916–921.

[126] W. Yang, Y. Yu, M.B. Starr, X. Yin, Z. Li, A. Kvit, S. Wang, P. Zhao, X. Wang, Ferroelectric polarization-enhanced photoelectrochemical water splitting in TiO_2–$BaTiO_3$ core–shell nanowire photoanodes, Nano Lett. 15 (2015) 7574–7580.

[127] A.A. Iyer, E. Ertekin, Asymmetric response of ferroelectric/metal oxide heterojunctions for catalysis arising from interfacial chemistry, Phys. Chem. Chem. Phys. 19 (2017) 5870–5879.

[128] J.H. Lee, A. Selloni, TiO_2/ferroelectric heterostructures as dynamic polarization-promoted catalysts for photochemical and electrochemical oxidation of water, Phys. Rev. Lett. 112 (2014) 196102.

[129] N. Nuraje, X. Dang, J. Qi, M.A. Allen, Y. Lei, A.M. Belcher, Biotemplated synthesis of perovskite nanomaterials for solar energy conversion, Adv. Mater. 24 (2012) 2885–2889.

[130] H. Yu, S. Ouyang, S. Yan, Z. Li, T. Yu, Z. Zou, Sol–gel hydrothermal synthesis of visible-light-driven Cr-doped $SrTiO_3$ for efficient hydrogen production, J. Mater. Chem. 21 (2011) 11347–11351.

[131] J. Liu, Y. Sun, Z. Li, S. Li, J. Zhao, Photocatalytic hydrogen production from water/methanol solutions over highly ordered Ag–SrTiO 3 nanotube arrays, Int. J. Hydrogen Energy 36 (2011) 5811–5816.

[132] H.W. Kang, S.N. Lim, S.B. Park, Co-doping schemes to enhance H_2 evolution under visible light irradiation over $SrTiO_3$: Ni/M (M= La or Ta) prepared by spray pyrolysis, Int. J. Hydrogen Energy 37 (2012) 5540–5549.

[133] Y. Zhong, K. Ueno, Y. Mori, X. Shi, T. Oshikiri, K. Murakoshi, H. Inoue, H. Misawa, Plasmon-assisted water splitting using two sides of the same $SrTiO_3$ single-crystal substrate: conversion of visible light to Chemical energy, Angew. Chem. Int. Ed. 53 (2014) 10350–10354.

[134] Y. Chang, K. Yu, C. Zhang, Z. Yang, Y. Feng, H. Hao, Y. Jiang, L.-L. Lou, W. Zhou, S. Liu, Ternary CdS/Au/3DOM-$SrTiO_3$ composites with synergistic enhancement for hydrogen production from visible-light photocatalytic water splitting, Appl. Catal. B Environ. 215 (2017) 74–84.

[135] Z. Jiao, T. Chen, J. Xiong, T. Wang, G. Lu, J. Ye, Y. Bi, Visible-light-driven photoelectrochemical and photocatalytic performances of Cr-doped $SrTiO_3$/TiO_2 heterostructured nanotube arrays, Sci. Rep. 3 (2013).

[136] H. Kato, M. Hori, R. Konta, Y. Shimodaira, A. Kudo, Construction of Z-scheme type heterogeneous photocatalysis systems for water splitting into H_2 and O_2 under visible light irradiation, Chem. Lett. 33 (2004) 1348–1349.

[137] K. Sayama, K. Mukasa, R. Abe, Y. Abe, H. Arakawa, A new photocatalytic water splitting system under visible light irradiation mimicking a Z-scheme mechanism in photosynthesis, J. Photochem. Photobiol. A Chem. 148 (2002) 71–77.

[138] P. Zhou, J. Yu, M. Jaroniec, All-solid-state Z-scheme photocatalytic systems, Adv. Mater. 26 (2014) 4920–4935.

[139] Y. Sasaki, H. Kato, A. Kudo, [Co (bpy) 3] 3+/2+ and [Co (phen) 3] 3+/2+ electron mediators for overall water splitting under sunlight irradiation using Z-scheme photocatalyst system, J. Am. Chem. Soc. 135 (2013) 5441–5449.

[140] Q. Jia, A. Iwase, A. Kudo, $BiVO_4$-Ru/$SrTiO_3$:Rh composite Z-scheme photocatalyst for solar water splitting, Chem. Sci. 5 (2014) 1513–1519.

[141] Q. Wang, Y. Li, T. Hisatomi, M. Nakabayashi, N. Shibata, J. Kubota, K. Domen, Z-scheme water splitting using particulate semiconductors immobilized onto metal layers for efficient electron relay, J. Catal. 328 (2015) 308–315.

[142] Q. Wang, T. Hisatomi, Q. Jia, H. Tokudome, M. Zhong, C. Wang, Z. Pan, T. Takata, M. Nakabayashi, N. Shibata, Y. Li, I.D. Sharp, A. Kudo, T. Yamada, K. Domen, Scalable water splitting on particulate photocatalyst sheets with a solar-to-hydrogen energy conversion efficiency exceeding 1%, Nat. Mater 15 (2016) 611–615.

[143] J. Brillet, J.-H. Yum, M. Cornuz, T. Hisatomi, R. Solarska, J. Augustynski, M. Graetzel, K. Sivula, Highly efficient water splitting by a dual-absorber tandem cell, Nat. Photonics 6 (2012) 824–828.

[144] M.S. Prévot, K. Sivula, Photoelectrochemical tandem cells for solar water splitting, J. Phys. Chem. C 117 (2013) 17879–17893.

[145] M. Graetzel, J. Augustynski, Tandem cell for water cleavage by visible light, in: Google Patents, 2005.

[146] Gurudayal, D. Sabba, M.H. Kumar, L.H. Wong, J. Barber, M. Grätzel, N. Mathews, Perovskite–hematite tandem cells for efficient overall solar driven water splitting, Nano Lett. 15 (2015) 3833–3839.

[147] J. Luo, J.-H. Im, M.T. Mayer, M. Schreier, M.K. Nazeeruddin, N.-G. Park, S.D. Tilley, H.J. Fan, M. Grätzel, Water photolysis at 12.3% efficiency via perovskite photovoltaics and Earth-abundant catalysts, Science 345 (2014) 1593–1596.

[148] S. Park, W.J. Chang, C.W. Lee, S. Park, H.-Y. Ahn, K.T. Nam, Photocatalytic Hydrogen Generation from Hydriodic Acid Using Methylammonium Lead Iodide in Dynamic Equilibrium with Aqueous Solution, vol. 2, 2016, p. 16185.

[149] B. Modak, P. Modak, S.K. Ghosh, Efficient strategy for enhancement of visible light photocatalytic activity of $NaTaO_3$ by a significant extent, J. Phys. Chem. C 121 (2017) 12980–12990.

[150] B. Modak, K. Srinivasu, S.K. Ghosh, Photocatalytic activity of $NaTaO_3$ doped with N, Mo, and (N,Mo): a hybrid density functional study, J. Phys. Chem. C 118 (2014) 10711–10719.

[151] C.-C. Hu, H.-H. Huang, Y.-C. Huang, N-doped NaTaO3 synthesized from a hydrothermal method for photocatalytic water splitting under visible light irradiation, J. Energy Chem. 26 (2017) 515–521.

[152] F. Gao, Y. Yuan, K. Wang, X. Chen, F. Chen, J. Liu, Z. Ren, Preparation and photoabsorption characterization of $BiFeO_3$ nanowires, Appl. Phys. Lett. 89 (2006) 102506–102900.

[153] J. Luo, P.A. Maggard, Hydrothermal synthesis and photocatalytic activities of $SrTiO_3$-coated Fe_2O_3 and $BiFeO_3$, Adv. Mater. 18 (2006) 514–517.

[154] U.A. Joshi, J.S. Jang, P.H. Borse, J.S. Lee, Microwave synthesis of single-crystalline perovskite $BiFeO_3$ nanocubes for photoelectrode and photocatalytic applications, Appl. Phys. Lett. 92 (2008) 242106.

[155] S.J. Moniz, S.A. Shevlin, D.J. Martin, Z.-X. Guo, J. Tang, Visible-light driven heterojunction photocatalysts for water splitting–a critical review, Energy Environ. Sci. 8 (2015) 731–759.

[156] H. Lu, Z. Du, J. Wang, Y. Liu, Enhanced photocatalytic performance of Ag-decorated $BiFeO_3$ in visible light region, J. Sol-Gel Sci. Technol. 76 (2015) 50–57.

[157] E. Grabowska, Selected perovskite oxides: characterization, preparation and photocatalytic properties—a review, Appl. Catal. B Environ. 186 (2016) 97–126.

[158] C. Pan, T. Takata, M. Nakabayashi, T. Matsumoto, N. Shibata, Y. Ikuhara, K. Domen, A complex perovskite-type oxynitride: the first photocatalyst for water splitting operable at up to 600 nm, Angew. Chem. 127 (2015) 2998–3002.

[159] W.L. Warren, D. Dimos, R.M. Waser, Degradation mechanisms in ferroelectric and high-permittivity perovskites, MRS Bull. 21 (1996) 40–45.

[160] G. Niu, X. Guo, L. Wang, Review of recent progress in chemical stability of perovskite solar cells, J. Mater. Chem. A 3 (2015) 8970–8980.

[161] T. Okada, T. Yagi, D. Nishio-Hamane, High-pressure phase behavior of $MnTiO_3$: decomposition of perovskite into MnO and $MnTi_2O_5$, Phys. Chem. Minerals 38 (2011) 251–258.

[162] X.H. Zheng, Z.H. Ma, P.J. Chen, D.P. Tang, N. Ma, Decomposition behavior and dielectric properties of Ti-doped $BiFeO_3$ ceramics derived from molten salt method, J. Mater. Sci. Mater. Electron. 23 (2012) 1533–1537.

[163] M. Akaogi, K. Abe, H. Yusa, H. Kojitani, D. Mori, Y. Inaguma, High-pressure phase behaviors of $ZnTiO_3$: ilmenite–perovskite transition, decomposition of perovskite into constituent oxides, and perovskite–lithium niobate transition, Phys. Chem. Minerals 42 (2015) 421–429.

[164] Z. Song, S.C. Watthage, A.B. Phillips, G.K. Liyanage, R.R. Khanal, B.L. Tompkins, R.J. Ellingson, M.J. Heben, Investigation of Degradation Mechanisms of Perovskite-based Photovoltaic Devices Using Laser Beam Induced Current Mapping, 2015, pp. 956107–956108.

[165] W. Liu, C.A. Randall, Thermally stimulated relaxation in Fe-doped $SrTiO_3$ systems: II. Degradation of $SrTiO_3$ dielectrics, J. Am. Ceram. Soc. 91 (2008) 3251–3257.

[166] Y. Cao, J. Shen, C. Randall, L.-Q. Chen, Effect of ferroelectric polarization on ionic transport and resistance degradation in $BaTiO_3$ by phase-field approach, J. Am. Ceram. Soc. 97 (2014) 3568–3575.

[167] S. Rodewald, J. Fleig, J. Maier, Resistance degradation of iron-doped strontium titanate investigated by spatially resolved conductivity measurements, J. Am. Ceram. Soc. 83 (2000) 1969–1976.

[168] Q. Ma, B. Iwanschitz, E. Dashjav, A. Mai, F. Tietz, H.-P. Buchkremer, Electrochemical performance and stability of electrolyte-supported solid oxide fuel cells based on Y-substituted $SrTiO_3$ ceramic anodes, Solid State Ionics 262 (2014) 465–468.

[169] T.A. Berhe, W.-N. Su, C.-H. Chen, C.-J. Pan, J.-H. Cheng, H.-M. Chen, M.-C. Tsai, L.-Y. Chen, A.A. Dubale, B.-J. Hwang, Organometal halide perovskite solar cells: degradation and stability, Energy Environ. Sci. 9 (2016) 323–356.

[170] S. Hu, M.R. Shaner, J.A. Beardslee, M. Lichterman, B.S. Brunschwig, N.S. Lewis, Amorphous TiO_2 coatings stabilize Si, GaAs, and GaP photoanodes for efficient water oxidation, Science 344 (2014) 1005–1009.

[171] M. Wang, L. Cai, Y. Wang, F. Zhou, K. Xu, X. Tao, Y. Chai, Graphene-draped semiconductors for enhanced photocorrosion resistance and photocatalytic properties, J. Am. Chem. Soc. 139 (2017) 4144–4151.